



Institute for Atmospheric and Earth System Research

Master's thesis
Master's Programme in Atmospheric Sciences
Geophysics of the Hydrosphere

Mixing processes under seasonal ice cover in boreal lake Kuivajärvi

Joonatan Ala-Könni
October 17, 2019

Supervisor: Ivan Mammarella
Reviewers: Petteri Uotila & Ivan Mammarella

UNIVERSITY OF HELSINKI
INAR – Institute for Atmospheric and Earth System Research

PL 64 (Gustaf Hällströmin katu 2)
00014 Helsingin yliopisto

Tiedekunta — Fakultet — Faculty		Koulutusohjelma — Utbildningsprogram — Degree programme	
Faculty of Science		Master's programme in Atmospheric Sciences Geophysics of the Hydrosphere	
Tekijä — Författare — Author			
Joonatan Ala-Könni			
Työn nimi — Arbetets titel — Title			
Mixing processes under seasonal ice cover in boreal lake Kuivajärvi			
Työn laji — Arbetets art — Level		Aika — Datum — Month and year	
Master's thesis		October 17, 2019	
		Sivumäärä — Sidantal — Number of pages	
		43	
Tiivistelmä — Referat — Abstract			
<p>Mixing processes under a seasonal ice cover in boreal lakes have received little attention from the physical limnological community. Even though the water is calm under the ice cover, many different phenomena are still able to cause mixing in the water column, which in turn affects the gas fluxes as well as physical and chemical properties of the water. Lakes in the boreal zone are very numerous. Understanding their behaviour helps us predict the effects of climate change in the boreal zone.</p> <p>In my thesis I present the various mechanisms that reign under the ice cover, and attempt to see these mechanisms in action in lake Kuivajärvi. Emphasis was placed on internal waves and the various components of the energy balance that can induce mixing. Data was collected with thermistor chains and a measurement raft between 24.1. – 3.5.2017.</p> <p>Two types of internal waves were observed during the ice-on season of 2016–2017. Short period barotropic seiches were observed during the whole ice-on season and transient long period baroclinic seiches were observed on two occasions. Other mixing processes seen in the lake were sediment heating in the dead of winter, penetrative convection caused by short wave radiation in the spring and diurnal stratification and mixing during spring caused by the daily heating and nightly cooling.</p> <p>Some mixing under the ice cover was found to depend on the meteorological conditions prevailing over the lake during the previous summer and just before the ice-on in late autumn, while others were more predictable. Long period internal waves and sediment heating are set in motion by meteorological conditions, while the spring mixing and overturn are more stable, due them being more a function of the orbital mechanics of our planet than the prevailing weather.</p> <p>Varying surface conditions of the lake ice cover make the measurement of especially the surface temperature complicated. Snow and ice are under a continuous metamorphosis due to the weather. This makes surface emissivity difficult to estimate, causing significant errors in the measurement of the outgoing longwave radiation. This in turn causes problems in defining the surface temperature from it. Also, the precipitation heat flux is difficult to estimate due to the lack of knowledge on the surface temperature.</p>			
Avainsanat — Nyckelord — Keywords			
physical limnology, hydrology, energy balance, internal waves, seiche, boreal lake			
Säilytyspaikka — Förvaringsställe — Where deposited			
Kumpula campus library			
Muita tietoja — Övriga uppgifter — Additional information			

- *Tämä on vettä.*
- *No niin ilmeisesti on!*

- *This is water.*
- *Well so it indeed seems to be!*

Geophysicists working on the field in Moominvalley (ep. 46, 'Hot springs')

Contents

1	Introduction	1
2	Theory	2
2.1	Boreal lakes and their characteristics	2
2.2	Lake thermal structure and its seasonal characteristics	2
2.3	Boundary layers above and below the surface	3
2.4	Lake surface energy balance	4
2.4.1	Water heat content	5
2.4.2	Radiation balance	5
2.4.3	Turbulent fluxes	8
2.4.4	Sediment heat flux	10
2.5	Mixing processes under ice	11
2.5.1	River inflow	11
2.5.2	Radiation in winter	11
2.5.3	Diffusion currents	12
2.5.4	Momentum exchange with the atmosphere	13
2.5.5	Internal waves in the ice-on season	14
2.5.6	Effect of Earth's rotation	15
3	Site and methods	17
3.1	Site	17
3.2	Instrumentation	17
3.3	Data analysis	19
4	Results	21
4.1	Meteorological conditions	21
4.2	Internal waves	21
4.3	Radiation balance	28
4.3.1	Shortwave radiation and albedo	28
4.3.2	Longwave radiation	30
4.4	Turbulent fluxes	32
4.5	Sediment heat flux	33
4.6	Thermal conditions and stability of the water column	34
4.7	Diurnal mixing in spring	36
4.8	Energy balance	37
4.9	Ice thickness	39
4.10	Precipitation heat flux	40
5	General discussion	40

List of Figures

1	Components of surface energy balance over a seasonally ice covered lake. . .	5
2	Saanajärvi with a layer of fresh snow.	7
3	Saanajärvi with a layer of old snow.	8
4	Two-layer gyre under ice.	13
5	Representation of different internal wave modes.	16
6	A map of the Kuivajärvi area.	18
7	Meteorological conditions over lake Kuivajärvi between 24.1. - 3.5.2017. . .	22
8	Wind rose.	23
9	Fourier spectrogram of the $z = 0.5$ m thermistor.	23
10	A fourier transform of the first 20 days of observations with surface seiches.	24
11	Wavelet transform of the first wave event.	25
12	Wavelet transform of the second wave event.	25
13	Comparison of the two baroclinic wave events.	27
14	Comparison of the isotherm data from the mid-winter (DOY 23 – 60) . . .	27
15	Comparison of the isotherm data from the spring (DOY 61 – 123)	28
16	Satellite image of cracks in ice cover of Kuivajärvi.	29
17	Shortwave radiation (Q_s , Q_r and net SW) over lake Kuivajärvi.	29
18	Albedo over lake Kuivajärvi.	30
19	Diurnal variation of albedo.	31
20	Incoming, outgoing and net longwave radiation.	31
21	Sensible and latent heat fluxes.	32
22	Comparison of EC and bulk aerodynamic method.	33
23	Sediment heat flux and temperature in the sediment during the ice-on season.	34
24	The evolution of the water column temperature and density profiles.	35
25	The evolution of water column heat content.	36
26	Example 1 of diurnal mixing.	37
27	Example 2 of diurnal mixing.	38
28	Surface energy balance of lake Kuivajärvi during ice-on season 2016 – 2017.	38
29	Comparison of calculated, measured and modeled ice thicknesses.	39

List of Tables

1	Typical values of emissivity for various surfaces.	6
2	Composition of the lake Kuivajärvi catchment area.	17

1 Introduction

Research on the physical phenomena occurring in and forcing on lakes has been concentrated mostly towards the open water season. However, majority of the lakes of the world are in climate zones where they have a seasonal ice cover. Until quite recently, for example, it was thought that biological activity was essentially nonexistent under the ice cover, but more recent research has shown that reality is far from this (Hampton et al., 2017). The ice cover does not isolate the lake completely from its surroundings, and the physical phenomena, especially in-lake mixing processes still have an effect on the gas fluxes and energy balance of the lake. Lakes have a major effect on the local environment, due to their properties being drastically different from the surrounding land.

Lakes affect the local climate through their large heat and water capacity, evening out the extremes. Lakes act as heat sinks during the summer, absorbing solar radiation into their often dark and murky waters. Heat is slowly released in the autumn, and the opposite is true in the spring, when a large amount of solar radiation is required to heat the lake to a strong summer stratification again. Lakes also act as a source of moisture, and thus have an effect on both the liquid precipitation and the snowfall of their surrounding area.

The effect of lakes on local climate is especially felt in the boreal and Arctic zones, where lakes can comprise a significant portion of the total surface area. These areas include large parts of Siberia, Northern America and Northern Europe. These areas also happen to be the subject of some of the most extreme heating under the climate change (Lee, 2014). Through an effect called *polar amplification*, the yearly mean temperature is projected to rise several degrees during this century. This directly affects, for example, the length of the ice season which is a very sensitive parameter in lakes with seasonal ice cover, and the temperature stratification of lakes. This in turn has an effect on the biology of the lake, on which many local communities depend their livelihoods on. For example, ice-roads provide a very useful connection for many communities during the winter. If *rasputitsa*, the period when ice prevents boating but is not strong enough to support any other mode of transport, mobility in winter suffers especially in remote communities. Also, on ice recreational activities, such as ice fishing, skiing or ice skating are held dear by the local people and tourist alike.

The biology and physics of lakes under ice cover has not received even nearly as much attention as has the ice-off season (Hampton et al., 2017), and especially internal wave activity under ice has not been studied very much at all. When ice insulates the usually dominating forces acting on the lake, wind and solar radiation, whatever is left has to be the dominant force driving currents and mixing. These are internal waves, diffusion currents and sediment heating. Mixing from such phenomena has an effect on the living conditions under the ice, and also affects gas fluxes during and after the ice-on season.

Of these mixing processes, especially basin scale baroclinic internal waves have received little attention (Kirillin et al., 2012). They are known to exist under ice, and due to the very weakly stratified nature of the water column, the waves can have a very significant amplitude even when the energy they contain is very small. They have been shown to cause significant mixing upon breaking during the open water season, especially in the shallow near shore areas, where the biological activity is also the highest.

In my thesis I aim to shed some light onto the physical conditions of the lake under a seasonal ice cover, by discerning the different components of the energy balance and by looking at what mixing phenomena reign under the seemingly immobile cover of ice. The data used as a basis for my research was collected during the winter 2016 – 2017 on boreal lake Kuivajärvi in Southern Finland, near the University of Helsinki Hyytiälä Forestry Station and the Institute of Atmospheric and Earth System Research (INAR) SMEAR II station.

2 Theory

2.1 Boreal lakes and their characteristics

Boreal lakes are mostly formed in depressions left behind by the last ice age. They are very prevalent in Canada, Alaska, Nordic countries and much of Russia. They are often surrounded by forest, comprising of either pine, spruce, birch, larch or a combination of these. Humic substances (also called Colored Dissolved Organic Matter, or CDOM for short) dissolving from the surrounding forest floor give many of these lakes a characteristic brown/yellow color, although they can also be very clear, especially on higher latitudes. In Finnish lakes, Secchi depths (which essentially is the visibility in water for the human eye) vary between 0.5 m and 10 m.

2.2 Lake thermal structure and its seasonal characteristics

Lakes that have a seasonal ice cover are in vast majority of cases dimictic, meaning that they undergo two complete overturns in a given year, one in the spring and one in the autumn. The rest of the year they are stably stratified. Density of water is a function of temperature, salinity and pressure, as is described by the TEOS-10 equation of state of water (IOC, 2010). As most boreal lakes are shallow and have a very low content of dissolved salts, salinity and pressure can be neglected, and the density of water can be assumed to be dependent only on temperature.

Due to temperature of maximum density of water being at $T_{MD} = +4\text{ °C}$, stratification changes on each overturn. When the lake cools in the autumn, it will eventually reach a temperature of maximum density from top to bottom, and then wind will very easily cause mixing in the whole water column. The lake stays isothermal, cooling down

further. The amount of cooling that happens during this period of the overturn depends on the dimensions of the lake basin and on the wind conditions in late autumn and early winter. If winds persist, cooling can happen all the way to $+1\text{ }^{\circ}\text{C}$. If the wind is calm, the water on the surface can stratify. This is because cooling happening below the temperature of maximum density makes the water less dense. One way or the other, if there is sufficient cooling the temperature of the surface water reaches freezing point, and the first ice appears. Supercooling of the surface water can occur, if the wind conditions are sufficiently calm and the water has very little freezing nuclei in it.

After the freezing, the water below the ice cover gains a stable stratification. Water just below the ice is at freezing point, and the temperature increases rather rapidly below it to around $+1\text{ }^{\circ}\text{C}$ within one meter of depth. This is the winter thermocline. Below it, is a weakly stratified layer, which ends near the bottom, where the temperature grows more rapidly towards the temperature of maximum density. Here, sediment heating makes the water warmer, and thus more stable. If the water would reach temperatures over the temperature of maximum density, it would immediately get mixed with the colder water above it, and thus the stratification is kept stable.

Snow cover is a very effective way to keep solar heating away from the lake. In this period, the water is at its quietest. When the spring progresses, sun climbs higher every day in the sky, and more heating gets through the snow and ice cover into the water. The surface water heats up, and thus gets denser. This forces it to mix with the water below it, creating an isothermal surface layer. The depth of this layer is made greater every day, as more heating is available. This continues up until the whole water column has reached the temperature of maximum density, and the spring overturn occurs. This overturn can happen before or after ice-off, and continue for some time, even weeks, depending on the wind conditions.

Summer stratification starts to build up as the whole water column is above the temperature of maximum density. Increasing temperature here means smaller density, and thus warmer water will be on the surface, and the water at $+4\text{ }^{\circ}\text{C}$ will again be on the bottom. The temperature of the surface water will follow the daily mean temperature of air rather well, but upwelling and mixing might temporarily change this. The surface layer (first 1 – 10 meters, depending on the transparency of the water) in summer is mixed, followed by the summer thermocline, below which the temperature quickly goes down. Cooling of the surface water is the first sign of the upcoming autumn in a boreal lake, and the dimictic cycle can repeat itself again.

2.3 Boundary layers above and below the surface

A surface boundary layer is defined as the layer where any fluid in motion is able to 'feel' a solid boundary. This is due to the no slip condition, which postulates that movement

of fluid contacting a solid surface is halted. Flow velocity as a function of the distance from the solid surface is logarithmic in shape in the constant flux layer, i.e. the vertical transport can be assumed to be constant within it.

Lake under a seasonal ice cover has several boundary layers. From top to bottom, these are between the atmosphere and the ice cover, ice cover and water and water and sediment.

The lake ice surface is very smooth. This low roughness lets wind blow rather freely over the lake, packing and blowing snow evenly throughout the ice cover. Wind conditions on the lake affect how fresh snow accumulates on the lake: low wind allows for more snow to accumulate and thus can result in more snow ice and less congelation ice. The packing of snow can lead to lake water flooding on the ice cover. This first boundary layer is well into the turbulent regime. Turbulent fluxes (in addition to outgoing long wave radiation) help transport away the latent heat of freezing, conducted through the ice.

The second boundary layer in a boreal lake can be found under the ice / water interface. It is stably stratified in the early winter, with a relatively steep vertical density gradient. Then, water in this layer is in a laminar-turbulent transition zone, due to the very low flow velocity of the water (in the order of $10^{-4} - 10^{-3} \text{ m s}^{-1}$). The layer turns turbulent in spring, when the mixed layer starts to penetrate its way down the water column.

The third boundary layer above the sediment / water interface is also in the laminar-turbulent transition zone. The flow is slow due to the very low energy phenomena occurring in it, like sediment heating and diffusion currents. In this boundary layer there usually exists a weak chemocline: nutrients, salts and gases dissolve from the sediment into the water. Occasionally, internal waves can break in this boundary layer, and mix the dissolved solids and gases up in the water column.

2.4 Lake surface energy balance

Energy balance in boreal lakes is drastically different between the seasons. In the summer, the lake water absorbs nearly all the light it receives from the Sun, while in the winter a cover of fresh snow can reflect in excess of 90 % of the light given by the Sun shining just barely above the horizon, thus essentially insulating the water column from short wave radiation. Also, the ice cover affects the turbulent fluxes significantly, due to lower air temperatures and water content and that it takes more energy to sublimate ice than it takes to evaporate water.

The surface energy balance equation for a lake can be written as

$$\frac{dQ}{dt} = Q_s - Q_r + Q_{La} - Q_{L0} + Q_c + Q_e + Q_P + Q_{SH} + Q_{RI} \quad (1)$$

where Q is the heat storage of the lake, Q_s and Q_r are the incoming and outgoing solar radiation, respectively. Q_{La} and Q_{L0} are the atmospheric (incoming) and surface (outgo-

ing) long wave radiation. Q_c is the sensible heat flux, Q_e is the latent heat flux, Q_p is the precipitation heat flux, Q_{SH} is the sediment heat flux and Q_{RI} is the net heat transport by river in- and outflowing. All of these terms have different magnitudes in different seasons, each playing their own part in the seasonal cycle of the lake.

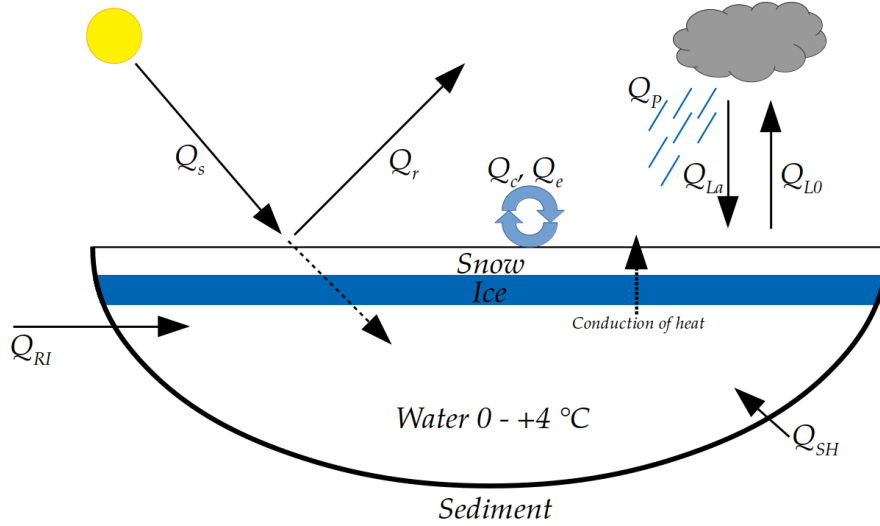


Figure 1: Components of the surface energy balance over a seasonally ice covered lake.

The properties of the energy balance define many key elements of the lake such as the ice-off and ice-on dates, the amount of primary production and the fluxes of gases. In the following sections the terms of the energy balance are explained.

2.4.1 Water heat content

The water acts like a thermal battery, due to the very high specific heat capacity of liquid water. In the heat content, the memory of the previous summer can be stored, which can affect the dynamics of the water under the ice cover.

The heat content of a water column can be characterized by the formula (Dijkstra, 2008)

$$Q = \int_{h_2}^{h_1} \rho(T, z) c_p(T, z) T(z) dz \quad (2)$$

where ρ is the density of water, c_p is the specific heat capacity of water, h_1 and h_2 are the top and bottom depths and $T(z)$ is the temperature of the water as a function of depth.

2.4.2 Radiation balance

All natural radiation that has an effect on a lake surface can be divided into two types: short wave and long wave, the first one coming from the Sun and the second one originating from the Earth. Thus, they are also known as solar and terrestrial radiation respectively. Both of these are approximately black body radiation (also called gray body radiation). Gray body radiation, also known as thermal radiation, is emitted by everything having

a temperature above the absolute zero, cold objects emitting at a longer wavelength and with a lower intensity radiation than their hotter counterparts.

The peak wavelength where a gray body radiator emits can be calculated by the Wien's displacement law:

$$\lambda_{max} = \frac{b}{T} \quad (3)$$

where $b = 2.898 \cdot 10^{-3}$ m K is the Wien's displacement constant and T is the temperature of the body. From here we can see, why the natural radiation on Earth can be divided into two classes. The peak wavelength for the average temperature of the Earth ($T \approx 14.6$ °C = 287.75 K) is $\lambda_{max} = 10^{-5}$ m. For the Sun ($T \approx 6000$ K) the peak is $\lambda_{max} = 4.83 \cdot 10^{-7}$ m. This is two orders of magnitude less, which means that these two types of radiation are easily discredited from one another.

The intensity of the radiation over the whole spectrum can be calculated by the Stefan - Boltzmann law:

$$M = \epsilon\sigma T^4 \quad (4)$$

where $\sigma = 5.670373 \cdot 10^{-8}$ W m⁻² K⁻⁴ is the Stefan - Boltzmann constant, T is the temperature of the surface and $0 \leq \epsilon \leq 1$ is the emissivity of the surface, which depends on the material properties of the surface in question.

Table 1: Typical values of emissivity for various surfaces.

Surface	Emissivity ϵ
Water	~ 0.95
Snow	~ 0.80
Ice	~ 0.96
Low clouds	~ 1
Frozen soil	~ 0.93

When measured in space around the Earth, the flux of radiation from the Sun can be considered as a constant on timescales relevant for this study. At a perpendicular angle and at the Earth's average distance from the Sun this so called solar constant has a value of $S_0 = 1367$ W m⁻². A fraction of this, around 30 - 80 %, is absorbed and scattered by the atmosphere and reflected from the clouds. Beyond the tropics of Cancer and Capricorn, in the high latitudes the Sun is never perpendicular to the surface, which limits the amount of radiation that reaches the surface due to geometry and the thicker atmosphere that the light has to travel through. The sum of all short wave radiation, scattered or direct, is the term Q_s in the equation (1). The ratio between scattered and direct radiation varies, depending on the cloudiness, aerosols and altitude of Sun from the horizon. Part of the short wave radiation is reflected upon hitting the surface. This is included in the term Q_r in Eq. (1), which is the sum of short wave radiation across all wavelengths reflected from the surface (Leppäranta, 2015).

From these two variables, the incoming and outgoing solar radiation, a very important

variable can be derived. Albedo describes the 'whiteness' of a given surface, by looking at the fraction of reflected sunlight to the total incoming solar radiation:

$$\alpha = \frac{S_{out}}{S_{in}} \quad (5)$$

Albedo thus receives values $0 \leq \alpha \leq 1$, and nearly the whole scale of values are found on surfaces of seasonally ice covered lakes during any given year. In the open water season albedo is very close to zero (~ 0.05), and thus the Sun heats the lake very efficiently with its radiation. Depending on the attenuation coefficient of the lake, solar radiation can penetrate the lake anywhere between under a meter in eutrophic lakes to over ten meters in some very clear spring fed lakes or tundra lakes.

On the other hand, fresh snow lying on the ice cover can have albedo values in excess of $\alpha = 0.9$. Combined with the fact, that around the time of the winter solstice at lake Kuivajärvi, the maximum altitude of the Sun in the sky is just 4.9° above the horizon, which means that radiation plays a very small role in the energy balance in mid-winter. For the largest part of the short day, the Sun is behind the tree canopy, and thus no direct sunlight is shining on the surface. During this period, other components of the energy balance dominate, namely the long wave radiation and turbulent fluxes.



Figure 2: Picture of lake Saanajärvi with a cover of fresh snow in March 2017.

A change in the surface albedo prompts a change in the energy balance. When the snow on the ice cover starts to melt due to short wave radiation increasing day by day, the snow grain size and the snow water content increase. This causes the surface albedo to decrease, and the snow cover gets a patchy, grey look to it. A positive feedback loop is initiated, where the melting snow grows in grain size and thus absorbs more light, which in turn is able to melt and grow the grain size even more and darkening the surface even further until the ice cover has completely melted (Leppäranta, 2015).



Figure 3: The same lake in June of the same year. A clear difference can be observed in the color of the snow cover, with the spring snow cover being patchy and significantly darker.

Terrestrial radiation is, as is the solar radiation, gray body radiation. But as the name 'terrestrial radiation' suggests, it is emitted by the Earth's surface and its atmosphere. The long wave radiation balance is typically in Finnish latitudes negative from October to March (surface loses heat), and positive (surface gains heat) from April to September (Leppäranta et al., 2017). According to the Stefan - Boltzmann's law (4), the typical range of emitted long wave radiation for the lake surface with an emissivity of $\epsilon = 0.96 - 0.97$ is in the range of $226 - 406 \text{ W m}^{-2}$ between temperatures of $-20 \text{ }^\circ\text{C} - +20 \text{ }^\circ\text{C}$. Depending on the atmospheric conditions (cloudiness, aerosols, temperature) a fraction of this is emitted back by the gray body radiation of the sky. During clear night skies, the long wave radiation is the most effective way of losing heat from a lake. On the other hand, a cloudy sky can insulate long wave radiation very efficiently and act like heat blanket, trapping the long wave radiation into the lower atmosphere.

2.4.3 Turbulent fluxes

The boundary layer of our atmosphere is in constant turbulent motion. It constitutes of eddies of different scales, and these whirls of air can transport heat, gases or particles with them. Two pathways for the generation of turbulence exist over a lake: thermal and mechanical. Thermal generation is prevalent, when the surface is warmer than the air above it, and convection begins. Mechanical generation of turbulence happens due to the no-slip condition (see section 2.3) at the boundary which generates shear, or in other words, vertical gradient of wind speed ($\frac{dU}{dz}$).

When studying a surface, one is interested in the vertical transport, i.e. what is taken out and what being deposited on the surface. This is the essence of the eddy covariance (EC) method. At its core is a three dimensional anemometer, capable of measuring the vertical component w of the wind at high rate (10 Hz). When combined with measurements of, for example air temperature, at the same time, the setup can keep track of heat going through and from the given surface. One can think of this like a

bouncer at the door of a nightclub, keeping tab of customers entering and leaving the club.

Contrary to other fluxes described here, turbulent fluxes are defined as entering to the surface when they are negative, and leaving the surface when they get positive values.

In the formulation of the turbulent fluxes, the fluctuating vertical component of the wind is defined as

$$w = \bar{w} + w' \quad (6)$$

where the wind speed w is defined as the sum of its 10 minute mean, \bar{w} , and fluctuation from that mean, w' .

Turbulent fluxes come in three types: sensible energy flux H , latent energy flux LE and momentum flux τ . Their magnitude is determined by the vertical wind speed, which in turn is dependent on the horizontal wind, and the value of the quantity in question (water vapor, heat, etc.) in a given parcel of air in an eddy.

Sensible energy, as the name suggests, holds in itself the transfer of heat in air that can be measured by a thermometer. It is defined as

$$H = \rho_a c_p \overline{w' \theta'} \quad (7)$$

where ρ_a is the density of air, c_p is the specific heat capacity of air, θ' is the fluctuation of potential temperature from the average and w' is the fluctuation of the vertical wind component. Essentially, what this is doing is keeping track of the heat that is transferred vertically through a given level above the ground via turbulent eddies.

Sensible heat flux gets its highest values when the temperature difference between the surface and the air above it is large. This happens, for example, when cold air is advected over a warmer surface, or vice versa, and when there is sufficient wind to mix the air over the surface.

Latent heat is the energy trapped in the phase change of water. During the ice-off period it is the evaporation or condensation of water from the surface, and in the ice-on season it is the sublimation or deposition of ice on the snow cover. It is defined as

$$LE = \rho_a L_{E/S} \overline{w' q'_a} \quad (8)$$

where L is either the latent energy of evaporation or sublimation (subscripts E and S , respectively), depending on the surface, and q'_a is the fluctuation of humidity.

For evaporation / sublimation to happen, there needs to be water to evaporate, heat for the evaporation and the air above the surface needs to be able to receive water (i.e., it can not be at saturation pressure). During winter, all of these conditions apply, but significantly less so than during the summer. Water is frozen, which increases the amount of heat needed for sublimation, not much heat is available and the air is cold and thus

not very capable of retaining vapor in it.

In places, where there is very little snowfall in the winter and where the air is dry and windy, a significant amount of ice can sublimate from the surface, if the surface just receives enough short wave radiation. Notably, these include places like the Antarctic and Tibet (Leppäranta, 2015) where the sublimation can reach over 10 cm for the winter. In the case of Finnish lakes the amount of sublimation is not discernible due to the drift of snow and the inaccuracies of measuring the snow and ice thicknesses, but it can be calculated to be in the order of a few millimeters.

Measuring the actual covariances found in the equations for turbulent heat fluxes (Eqs. (7) & (8)) is rather complicated, and requires sophisticated eddy covariance techniques. In many occasions, the fluxes would still be useful to estimate, in which case the bulk aerodynamic method comes into use. In it, the sensible (latent) heat flux is written as a function of wind speed and the temperature (humidity) difference between the air and the surface. Simpler measurements give then approximations on the flux. As described in (Leppäranta et al., 2017), they are written as

$$H = \rho_a c_a C_H (T_a - T_0) U \quad \text{and} \quad (9)$$

$$LE = \rho_a L_{E*} C_E (q_a - q_0) U \quad (10)$$

where ρ_a is the air density, c_a is the heat capacity of air, L_{E*} is the latent heat of evaporation or sublimation, $C_H \approx C_E \sim 1.5 \cdot 10^{-3}$ are the exchange coefficients of sensible and latent heat, respectively, and U is the wind speed.

2.4.4 Sediment heat flux

Sediment heating can cause mixing inside of a lake during the early winter. During the warm summer months heat is stored in the sediment, and this then gets slowly released back into the water during the ice-on season.

Thermal conduction happens as described by the Fourier's law of thermal conduction

$$\mathbf{q} = -k \nabla T \quad (11)$$

where \mathbf{q} is the heat flux through an unit area, k is the thermal conductivity of the given material and ∇T is the temperature gradient. Horizontal variation in temperature can be assumed to be small in the case of the sediment heating, and a one-dimensional form can be utilised

$$Q_{SH} = -k \frac{dT}{dz} \quad (12)$$

where z is the vertical coordinate.

During the winter stratification, when the whole lake temperature is below the density

maximum ($\sim+4$ °C), all heating in the water moves it closer to this temperature. Thus, water heated at the sediment / water interface gets more dense than the surrounding water. This causes a downward flow of water in the sediment / water interface, and an upward return current in the center of the lake. Research has shown that this can be a dominant mode of circulation in a lake during the early winter, but the effect is diminished as the heat from the sediment is lost and the difference in temperature equalizes. This happens typically in less than 60 days after the onset of the ice cover, depending on the conditions of the previous summer (Kirillin et al., 2012), (Rizk et al., 2014).

The magnitude of these currents is in the order of 10^{-4} m s⁻¹, which is enough for the current to be in geostrophic balance even in rather small lakes.

2.5 Mixing processes under ice

Mixing processes in lakes under ice cover differ significantly from the ice-off season. The ice cover acts as a very effective insulator of heat, and also of momentum and radiation. Solar radiation and wind drive mixing processes during the ice-off season, but in the winter as these are restricted, weaker processes take hold of the situation. Namely, sediment heating, diffusion circulation, river influx and internal waves.

2.5.1 River inflow

Shallow lakes that have a significant river flow-through during the winter can lose heat from their water body this way, as the lake water is constantly being replaced by the ~ 0 °C river water.

In deeper lakes the effect might be small, since the water at near freezing temperatures are less dense than the rest of the water column, and this light water might just skim over the lake, barely mixing or transporting heat at all.

2.5.2 Radiation in winter

Optical properties of ice and snow (together with the orbital parameters of our planet) control the radiation environment under the ice cover. These properties of lake ice cover depend on the type of ice. The ice formed from lake water, congelation ice, is formed of elongated ice crystals in the scale of 10^{-1} m in length and 10^{-2} m in width. Congelation ice is typically clear. On top of the congelation ice usually forms a layer of snow ice, which is formed by the thawing and refreezing of snow, precipitation and lake water. Its crystal size is much smaller, in the millimeter scale (10^{-3} m). This leads to a milky appearance of snow ice, which makes it optically significantly thicker than congelation ice. But the most efficient way to reflect and block light is snow. Even a few centimeters of snow effectively block nearly all light from penetrating the ice cover. This due to the high albedo of fresh snow ($\alpha = 0.8 - 0.9$) and also the scattering properties of snow due to the small crystal

size. Congelation ice can, on the other hand, be nearly as clear as pure water. The clarity of congelation ice depends on the number of gas bubbles trapped in the ice and the size of the crystals.

Insulation of the ice cover is the limiting factor of ice growth in lakes. This makes the growth of ice a typical negative feedback loop, where the phenomena itself is limiting its own growth.

In late winter — early spring, as the days get longer and the Sun lingers higher up over the horizon, more short wave radiation is able to penetrate the ice cover. This forces the topmost layer of water to convectively mix. When radiation is absorbed in the 0 °C water just below the ice, it gets denser and mixes with the water below it. Every passing day accumulates more heat into the water just below the ice, and thus the isothermal convecting layer gets deeper and deeper, until the whole body of water is at the temperature of the density maximum. Spring overturn has occurred at this point, and summer stratification starts to form, as water heated above the T_{MD} is less dense and thus always stays on top of the water column. In spring this stratification can still be so weak, that several overturns can take place in quick succession before a permanent stratification can form. The timing of the spring overturn varies less than the timing of the autumn overturn from year to year, due to the fact that it is dominated by the shortwave radiation, which in turn is controlled by the latitude of the lake. Sometimes the spring mixing happens during the ice-on period, thus potentially resulting in anoxia during the summer.

Salinity, or the lack of thereof, can influence the spring mixing. The meltwater can be almost completely depleted of dissolved matter, and therefore be less dense than the lake water. Conversely, the water at the sediment / water interface can be significantly saltier than the rest of the water column. If the salinity gradient is strong enough, this can lead to a situation where the penetrative convection does not reach throughout the whole water column. This can eventually make the lake meromictic, i.e. not completely mixing. Very fresh and thus less dense meltwater in the surface layer can cause a lake to become partially meromictic during the melting period, slowing down the onset of spring overturn.

During the period of penetrative convection, the nightly flux of heat through the ice out into the atmosphere in the form of long wave radiation causes a weak stratification to form in the convective layer. It collapses in the morning after short wave radiation enters the water again, leading to diurnal convective mixing in the topmost layer of the water column.

2.5.3 Diffusion currents

Mixing processes arising as a result of radiation are strong, but weaker phenomena still can cause mixing during the winter, when radiation is all but isolated from the water column.

As theoretically shown by (Phillips, 1970) and (Wunsch, 1970), stratified column of water can only be stable in a container with strictly vertical and parallel walls. If there is any inclination of the walls, as is typical for lakes, diffusion of heat due to the gradient caused by the stratification, a small horizontal pressure gradient is formed at the water – sediment boundary. According to the continuity equation, this results in an upward flow of water near the walls, and a downward return current in the center of the lake. Sometimes, when combined to the sediment heating in the early winter and the Coriolis force in a sufficiently large lake, two counter rotating gyres can form on top of each other: topmost being driven by the sediment heating and the lower one driven by the diffusion currents (Fig. 4) (Malm, 1999).

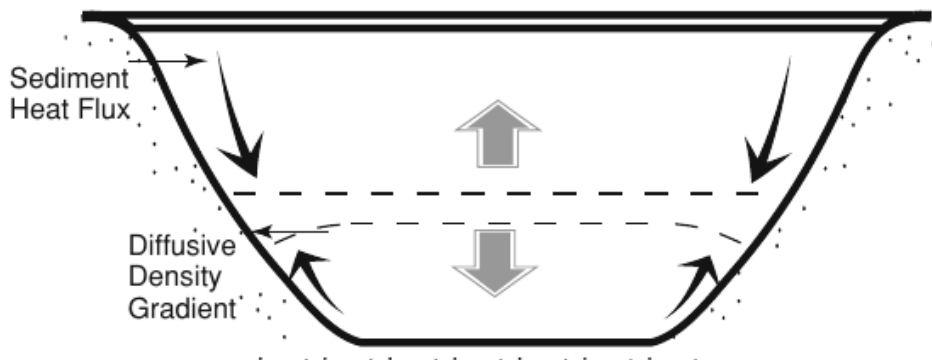


Figure 4: The two-cell circulation, showing the counterrotating gyres. (Kirillin et al., 2012)

2.5.4 Momentum exchange with the atmosphere

The nature of momentum exchange is also different in the ice-on season. In the open-water season wind drives the waves directly, but as with other exchanges, ice hampers this. Instead, the floating ice cover is tilted by the wind, and when this tilt restores, oscillations in the water can be induced. Also, differences in atmospheric pressure can drive oscillations, but this mostly applies to very large lakes, as the horizontal gradient of atmospheric pressure is always rather small (c. 10 Pa km^{-1}).

In the open-water season the nature of internal wave activity can be characterized by the Wedderburn number and Lake number, which describe the ratio between the wind stress on the lake surface and the strength of the stratification, and thus inform us on the level of thermocline tilt (Horn et al., 2001). Wedderburn number is defined for a two layer stratification, which for many cases is sufficient. It is defined as

$$W = \frac{g'h_1^2}{Lu_*^2} \sim \frac{h_1}{\eta_0} \quad (13)$$

where h_1 is the surface layer depth, η_0 is the initial displacement of the thermocline and $g' = \frac{\Delta\rho}{\rho}g$ is the reduced gravitational acceleration (where $\Delta\rho$ is the change in density over

the layer in question), which takes into account the buoyancy of the water, L is the length of the lake basin and u_* is the friction velocity. It can be written as

$$u_* = \sqrt{\frac{\tau}{\rho_a}} \quad (14)$$

where τ is the momentum flux, defined as

$$\tau = \rho_a \overline{u'w'}. \quad (15)$$

Lake number is a more general definition, that does not require a two layer stratification, but is also more complex to compute. But since both are defined through friction velocity u_* , which itself is defined at the water / atmosphere interface, this sort of classification does not function in the ice-on season without redefining it.

2.5.5 Internal waves in the ice-on season

Even though the surface of a lake looks calm and immobile in the dead of winter, the lake still has waves in it driven by the wind and changes in the atmospheric pressure. The lakes can give both a barotropic (affecting the whole water body) and baroclinic (waves moving along interfaces or in stratified fluid) response to forcing from the atmosphere.

Barotropic waves, also known as surface seiches are a well known property of lakes. An everyday observation comparable to this would be the oscillation of water in a bathtub when it is tilted. They are not inhibited by the ice cover, but their amplitude can be somewhat smaller in the winter (Kirillin et al., 2012). Their period can be predicted by the Merian's formula (Merian, 1828)

$$T_n = \frac{2L}{n\sqrt{gh}} \quad (16)$$

where L is the length of the lake, g is the gravitational acceleration, h is the average depth of the lake and n is the mode of the wave, so that the second mode has period half of the first one, the third mode has a period of one third of the first mode etc. Typical periods for small lakes are in the order of minutes to tens of minutes. The wave speed can be calculated from the shallow water wave theory

$$c = \sqrt{gh} \quad (17)$$

where g is the gravitational acceleration and h is the average depth of the lake.

Barotropic waves are standing waves, and the first seiche mode has one node at the center of the lake, second mode has one more node and so forth. In this sense, comparable phenomenon could be seen in the strings of some musical instruments, like a violin or a

guitar.

Baroclinic waves are not features of the whole lake, but rather propagate through the lake. They also have periods much longer than barotropic waves, in the order of several days. Due to their low velocities, they can also be subjected to the effects of Earth's rotation, something usually attributed to currents in much larger scales in the ocean and in the atmosphere.

For the case of the continuously stratified fluid, the speed of the wave gains the form presented in (Leppäranta, 2015)

$$c_i = \frac{1}{\pi}NH = \frac{H}{\pi} \sqrt{\frac{g}{H} \frac{\Delta\rho}{\rho_0}} \quad (18)$$

where H is the thickness of the stratified layer, $\rho_0 = 999.95 \text{ kg m}^{-3}$ is the reference density, $\Delta\rho$ is the change of density along this stratified layer and N is the *Brunt-Väisälä frequency*, which is defined as

$$N = \sqrt{-\frac{g}{\rho} \frac{d\rho}{dz}} \quad (19)$$

A period for a specific horizontal mode in a continuously stratified fluid can be computed with the formula

$$T_n = \frac{2\pi n}{\sqrt{\frac{g}{H} \frac{\Delta\rho}{\rho_0}}} \quad (20)$$

Baroclinic waves are induced by wind in the early winter, when the ice cover is still young and elastic. As the winter progresses, the ice cover gets thicker and more rigid. This means that the wind has less and less effect on the lake tilting. When the wind is not able to induce waves anymore, changes in the atmospheric pressure are still able to. Unlike the barotropic waves, baroclinic waves can induce mixing in the water when they break. The waves have a higher amplitude near the shores, where they are also more likely to break (Kirillin et al., 2009). The exact role of these internal waves in the under-ice mixing in lakes is not clear. In the heat balance the dissipation of these waves is not significant (Kirillin et al., 2012).

As with the surface seiche waves, baroclinic waves can have several different modes, both horizontally and vertically, as illustrated in figure 5. At least three vertical modes have been observed in the open water season (Vidal et al., 2005) when diurnally varying wind resonates with the lake.

2.5.6 Effect of Earth's rotation

Flows in both the atmosphere and in water bodies are affected by the rotation of the Earth. It seems as if a force is constantly applied to the fluid, while in reality it is just the Earth rotating under the fluid. For an observer in the rotating coordinate system of the Earth it looks as if the fluid is being acted upon. This pseudo force (i.e., not really

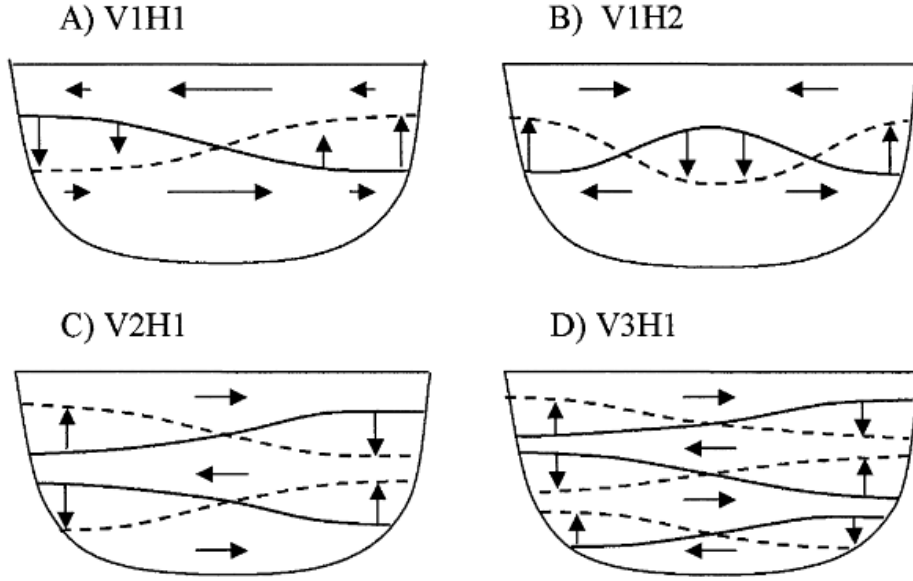


Figure 5: Schematic of four different internal wave modes. Arrows indicate the direction current associated with the wave and the solid and dashed lines indicate isotherms at the two extreme positions of the wave respectively (Vidal et al., 2005)

a force) is called the Coriolis force. If there is enough space and time for the flow, the Coriolis force will turn the flow into a circulation. The room required for this is called the Rossby radius of deformation, and it is defined by the formula

$$L_R = \frac{(gD)^{1/2}}{f} \quad (21)$$

where g is the gravitational acceleration, D is the characteristic depth and f is Coriolis parameter. This in turn is defined by the formula

$$f = 2\Omega \sin \phi \quad (22)$$

where ϕ is the latitude and $\Omega = 7.2921 \cdot 10^{-5} \text{ rad s}^{-1}$ is the rotation rate of the Earth.

All of the phenomena described above can be affected by the Earth's rotation if the lake is sufficiently large or if the current velocities are low. In the open water season a lake would have to be exceptionally large (at least tens of kilometers) and shallow (a few meters) for the Coriolis effect to be significant. Because current velocities in general are several orders of magnitude smaller than those in the summer, even lakes with diameters less than a kilometer can have Coriolis driven gyres in them (Malm, 1999). It has been observed that sediment heating creates one gyre and the diffusion currents create a second, counterrotating one below it with a quiet zone in the middle where the two forces are equal. For comparison, in the atmosphere jet streams can have Rossby radii in the order of thousands of kilometers, while under ice in an Arctic lake the Rossby radius can be in

the order of hundreds of meters.

Barotropic internal waves can develop two different types of responses for the rotation of the Earth: Kelvin and Poincaré. They are rotating waves, propagating themselves around the lake, like water in a glass being rotated by hand. Both types have been observed in lakes under seasonal ice cover (Kirillin et al., 2009).

3 Site and methods

3.1 Site

Lake Kuivajärvi is a dimictic, mesotrophic lake in Southern Finland (lon. 24° 16' E, lat. 61° 50' N, 141 m above mean sea level). It is located in the Kokemäenjoki water system, which drains into the Baltic Sea. The lake has a strongly elongated shape, 2.6 km in the north – south direction and 200 – 400 m in the east – west direction. The lake has two basins, the southern basin being the deeper one with a maximum depth of 13.2 m. The raft used for various measurements is located approximately on this deepest point. Lake Kuivajärvi is surrounded mostly by managed Scots pine forest, which is also the home for the SMEAR II station. Typical ice cover period in lake Kuivajärvi lasts for about five months, starting in late November – early December and ending in late April – early May. A mild decreasing trend in the length of the ice-on season has been observed here since the start of observations in 1929. The ice cover thickness at the start of the melting period is 40 – 50 cm (Korhonen, 2006).

Table 2: Composition of the lake Kuivajärvi catchment area as % of the catchment area ($A = 18.6 \cdot 10^6$ m²). Data: Finnish environment institute *SYKE*.

Dense forest	78.9 %
Sparse forest	11.2 %
Inland water	5.4 %
Bog	0.6 %
Agriculture	0.3 %
Other	3.6 %

3.2 Instrumentation

During the winter of 2016 – 2017, three RBR Concerto thermistor chains were in use. The recorded period was between 24.1.2017 – 3.5.2017. All of the chains were situated in the southern basin, and they were positioned every 50 meters. The northern and southern chains had 16 thermistors each, ranging in depth between 0.5 m and 12.4 m. In the middle chain, positioned 5 meters north of the raft, there were 15 thermistors ranging between 0.5 m and 10.4 m. The thermistors were set to record the temperature as a 60 s average.

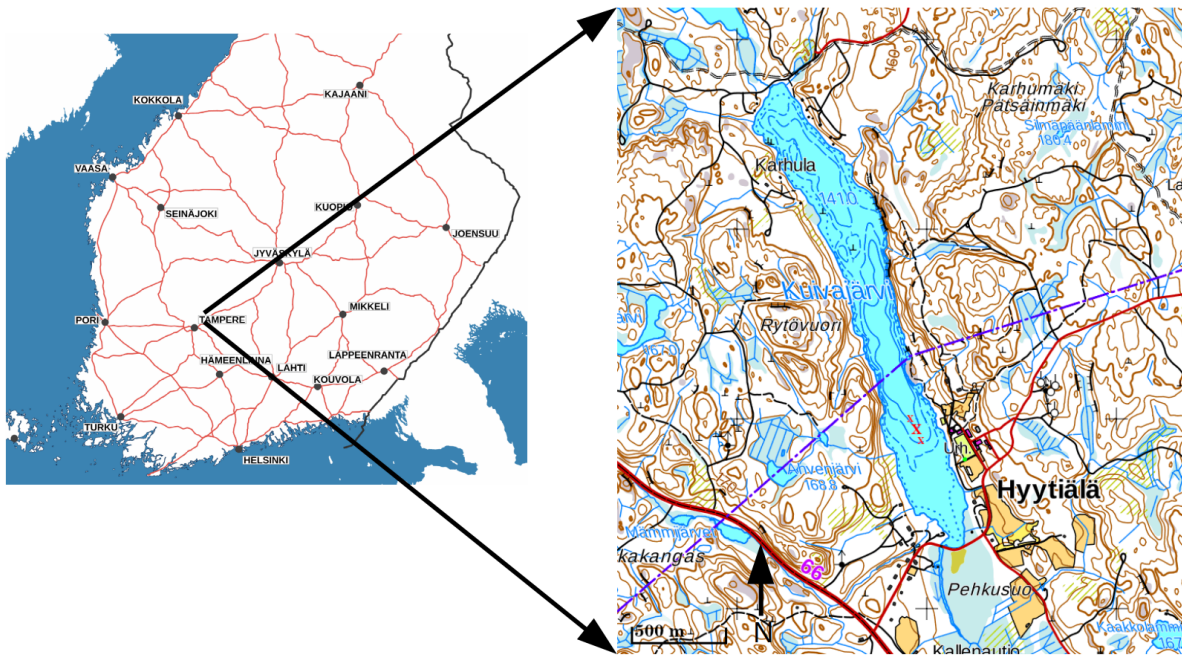


Figure 6: A map of the Kuivajärvi area and its location in Southern Finland. The three red crosses on the lake mark the locations of the thermistor chains. The biggest cross in the middle is the location of the raft and the associated chain. The location of the SMEAR II station is indicated by the four white circles east of the raft and chains. Map: National Land Survey of Finland.

A rig containing a total of eight thermistors was moored at the sediment to record the heat flux through the sediment. The top and bottom thermistors were RBR duet loggers, recording temperature and depth. The loggers in between were of RBR solo -type, only recording temperature. The thermistors were evenly spaced, every 5 cm. As with the thermistor chains, data was logged every minute.

Additional data is obtained from the raft on lake Kuivajärvi, as well as from the SMEAR II station (Hari & Kulmala, 2005). A Metek USA-1 3-axis anemometer provided the three component wind speed and sonic temperature above the lake. Turbulent flux measurements were complemented with a LiCor LI-7200 gas analyzer that measured the water vapor in air. A Kipp & Zonen CNR1 net radiometer and pyranometer was used to acquire the radiation balance. This single instrument measured both directions of the short wave (305 – 2 800 nm) and long wave (5 000 – 50 000 nm) radiation. The raft also contained an experimental sensor for detecting ice cover thickness and temperature. It consisted of a hundred thermistors and conductivity sensors spread over a one meter plastic rod. The data is averaged over a day. Air temperature was provided by a regular temperature sensor at the height of 2 m.

The SMEAR II station provided values for atmospheric pressure and precipitation. The tower containing the instruments was located less than 1 km from the raft, and results from there can be considered representative for the lake as well.

3.3 Data analysis

The thermistors recorded values every 60 s, which considering the time scale of the observed phenomena is enough, but barely. Nyquist's theorem states, that the time of the shortest wave period that still can be resolved with any sampling period is two times that sampling period (or half of the sampling frequency). The wave periods estimated by Merian's formula (16) were in the order of ten minutes or less, but no shorter than 2 minutes. An order of magnitude greater sampling frequency (~ 5 s) would have been more optimal, but in that case the response time of the thermistors might have caused noise in the data, which now was very clean of it. No filtering was done to the data, as all natural oscillations in the data seemed to be clear of artificial disturbances.

The calibration of the thermistors was in a good order, since they had been refurbished at the factory just before deployment, in the autumn of 2016. This resulted in very consistent values. Recorded values from individual thermistors were within 10^{-2} °C from each other during mixing events, when the whole water column can be expected to have a constant temperature.

Isotherms were created from the thermistor data by linear interpolation of the data. These isotherms, estimating the depth of a given temperature, were used to visually inspect and identify internal wave events for a more detailed harmonic analysis.

Two methods were used for the harmonic analysis: Fourier transform and wavelet analysis. Both essentially try to achieve the same thing, which is to discern periodicities in a given time series. Fourier transform is better suited for short periods (like the surface seiches in this case) and steady oscillations, while wavelet analysis is better suited for long periods (like the baroclinic seiches in this case) and non-steady or transient oscillations.

Fourier analysis was done by using fast fourier transform (*FFT* for short) in MatlabTM. Blackman-Harris windowing was applied, which is a commonly used window in geosciences. It provides with a small window leak in low frequencies, and a low constant leak for higher frequencies, and it is rather simple to see when this constant leak gets higher than the signal. This means that the noise generated by the process of FFT itself remains small, and it has a distinct shape that is easy to discern from the actual noise originating from the dataset itself.

For wavelet analysis, MatlabTM was also used. It contains the *cwt* function, which performs a continuous 1-D wavelet transform of a given data set.

Heat content of the lake was calculated according to equation (2). The integration was performed numerically using the trapezoidal method. Temperature at the ice / water interface was assumed to be 0 °C throughout the measurements. Density of water was calculated with a simplified formula, only taking into account the temperature and

assuming normal atmospheric pressure (Leppäranta et al., 2017) :

$$\begin{aligned} \rho_w = & 999.842594 + 6.793952 \cdot 10^{-2} \cdot T - 9.095290 \cdot 10^{-3} \cdot T^2 \\ & + 1.001685 \cdot 10^{-6} \cdot T^4 + 6.536332 \cdot 10^{-9} \cdot T^5, \end{aligned}$$

where T is the temperature in degrees of kelvin. As the specific heat capacity of water is also dependent on temperature, it was estimated with the formula (Cohen et al., 2003):

$$c_w = 4217.4 - 3.720283 \cdot T + 0.1412855 \cdot T^2 - 2.654387 \cdot 10^{-3} \cdot T^3 + 2.093236 \cdot 10^{-5} \cdot T^4,$$

where T is the temperature in Celsius.

In the estimation of the turbulent fluxes via the bulk aerodynamic method several calculations had to be made. In equations (9) and (10) on the air temperature T_a and humidity q_a are directly measured. The density of air was estimated with the ideal gas equation of state. The heat capacity of air was considered constant, $c_a = 1003.5 \text{ J kg}^{-1} \text{ K}^{-1}$. Latent energy of water was estimated with a formula (Rogers & Yau, 2014):

$$\text{For evaporation: } L_E = 2500.8 - 2.36 \cdot T_a + 0.0016 \cdot T_a^2 - 0.00006 \cdot T_a^3 \text{ J g}^{-1} \quad (23)$$

$$\text{For sublimation: } L_S = 2834.1 - 0.29 \cdot T_a - 0.004 \cdot T_a^2 \text{ J g}^{-1}, \quad (24)$$

where temperature is in Celcius. Surface humidity was assumed to always be at saturation point (Leppäranta et al., 2017). Saturation water mass fraction was estimated with (Puhakka & Bister, 1996):

$$q_s = RH \cdot 0.622 \left(\frac{Ae^{\frac{B}{T_a}}}{p_0} \right) \quad (25)$$

where $A = 2.53 \cdot 10^9 \text{ kPa}$, $B = 5.42 \cdot 10^3 \text{ K}$, RH is the relative humidity ($0 \leq RH \leq 1$) and p_0 is the atmospheric pressure. Temperature is in degrees of Kelvin.

Surface temperature was estimated with the Stefan-Boltzmann law (Eq. 4) and the measured outgoing longwave radiation. Constant emissivity of $\epsilon = 1$ was assumed.

For the modeling of the ice cover thickness the very rudimentary *Stefan-Zubov* model was used. It is based on the heat exchange between the ice cover surface and the atmosphere, and it assumes no snow cover, zero ice in the beginning and water temperature at freezing point at the ice / water interface. Several formulations of Stefan-Zubov model exist, but in (Leppäranta et al., 2017) it is presented as

$$h_i(t) = \sqrt{a^2 S + b^2} - b, \quad (26)$$

where $a \approx 3.3 \text{ cm } ^\circ\text{C}^{\frac{1}{2}} \text{ day}^{\frac{1}{2}}$, $b \approx 10 \text{ cm}$ and S is the sum of negative degree days. This means the sum of daily mean temperatures for such days, where this mean is below freezing. Similar model for melting can be applied (Leppäranta et al., 2017), but is not

used in this analysis.

4 Results

4.1 Meteorological conditions

Weather over lake Kuivajärvi during the winter of 2016 – 2017 was typical for Southern Finland (Fig. 7). Temperatures of above freezing were observed from late January onwards, but consistently the air was above freezing during the daytime after mid-March. Nightly freezing temperatures were seen all the way until ice-off in early May. Mean temperature for the whole period was -1.77 °C.

Wind tends to get directed by the channel that runs along the lake as can be seen from the wind rose (Fig. 8). This means that the wind blows roughly in the north-south direction over the lake. Typically, wind speed remained below 6 m s^{-1} , with only four events recorded that were clearly over this value. Peak wind speed was reached during a storm in late March, when a value of 11.6 m s^{-1} was measured, after which the sensor suffered a malfunction.

Relative humidity stayed for most of the time over 80 %, especially during the winter months. During the spring months relative humidity could plummet to lower values due to the Sun heating the air above the lake.

The winter months saw little precipitation, and most of that can be assumed to be snow. Precipitation became more prevalent during the spring months, and it also was more likely to be liquid. The sum of precipitation over the lake during the measurement campaign was 117 mm of liquid water equivalent.

4.2 Internal waves

In the ice-on season of 2016 – 2017 both baroclinic and barotropic seiches were observed throughout the winter. Short period, surface seiche waves of several different modes were observed, as is made clear by the fourier spectrogram plot (Fig. 9).

The main peak of the oscillations can be found at approximately $T = 660$ s. When comparing this with the value calculated from Merian’s formula (Eq. 16) with values $L = 2500$ m for the length of the lake and a mean depth of $h = 6$ m we get a value for the period of first mode basin scale seiche of $T_0 = 652$ s, which is very close to the measured main peak. All of the peaks stay at the same period throughout the winter.

In Fig. 9 also other horizontal lines can be seen. They become more apparent when plotting the fourier transform of a time period when seiching was more intense (Fig. 10).

Surface seiche modes at least from one through four can be observed at frequencies $f_1 \approx 1.4 \cdot 10^{-3}$ Hz, $f_2 \approx 2.8 \cdot 10^{-3}$ Hz, $f_3 \approx 3.9 \cdot 10^{-3}$ and $f_4 \approx 4.3 \cdot 10^{-3}$ Hz, respectively.

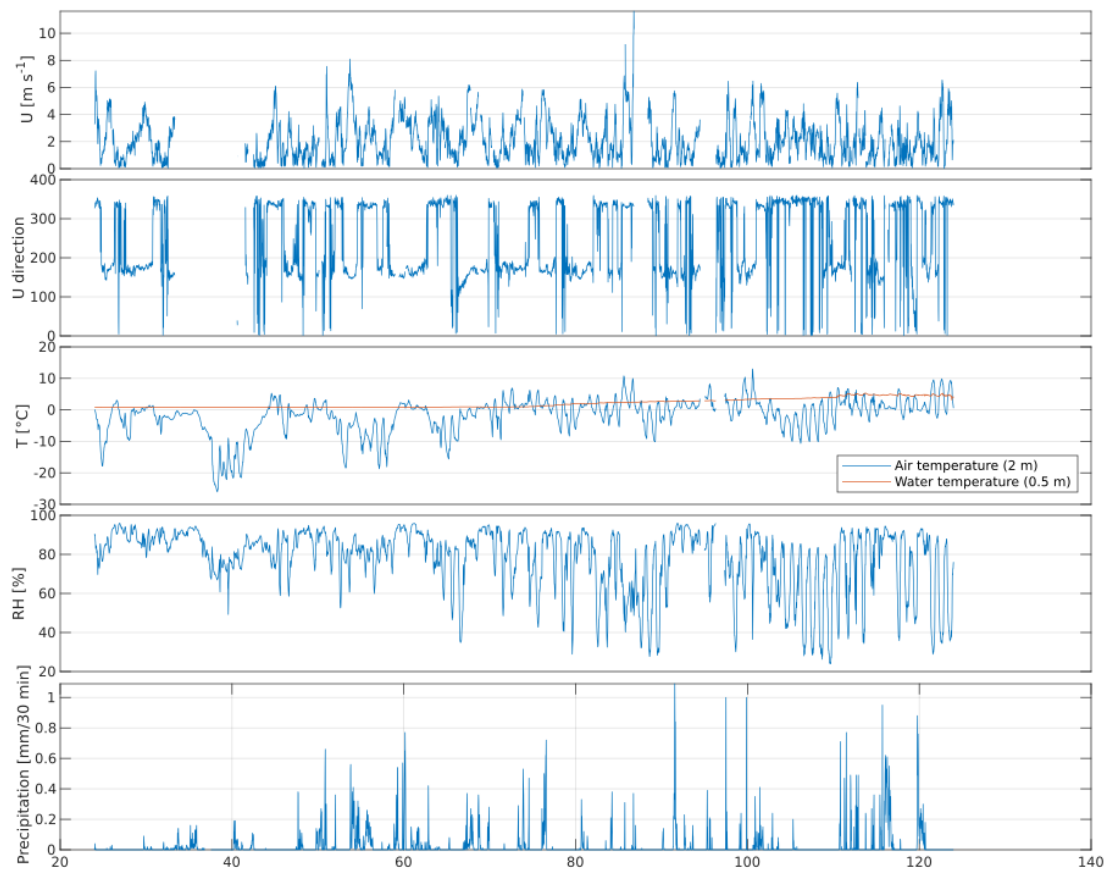


Figure 7: Meteorological conditions over lake Kuivajärvi during the ice-on season (24.1. - 3.5.2017). Precipitation is presented as a 30 minute sum of liquid water equivalent. All other variables are 30 minute average values.

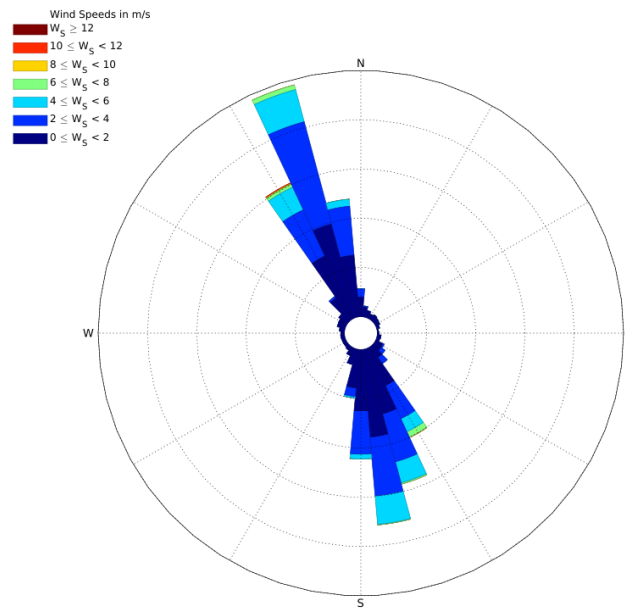


Figure 8: Wind rose, showing the strong channeling effect due to the topography of the terrain surrounding lake Kuivajärvi.

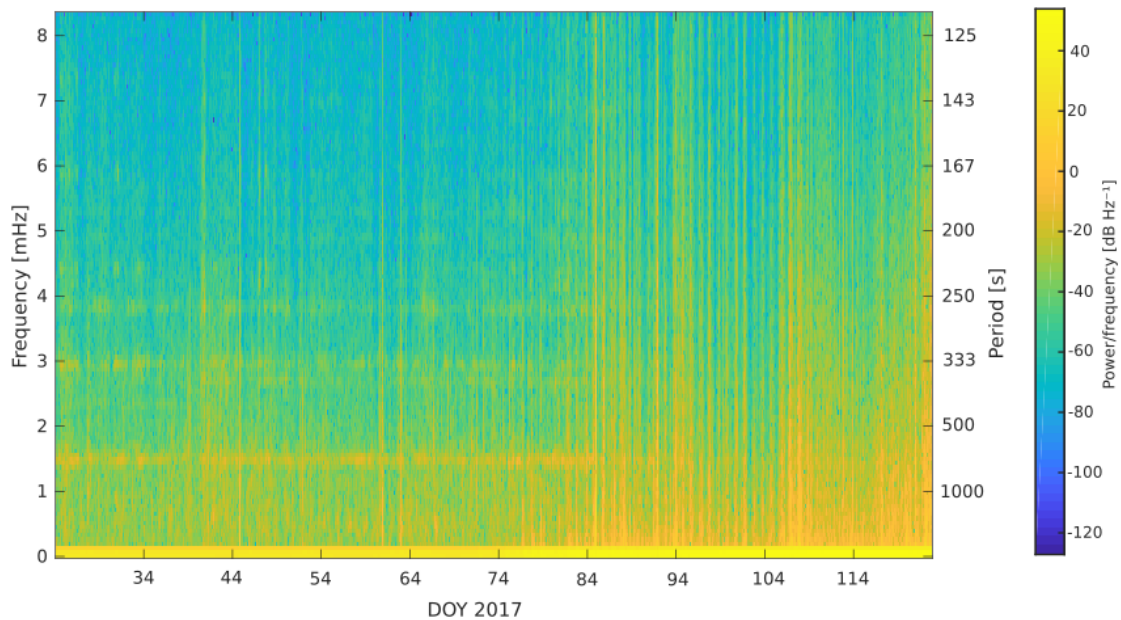


Figure 9: Fourier spectrogram of the uppermost thermistor ($z = 0.5$ m) from the northern chain. Seiche modes can be seen as horizontal yellow lines in the plot, spanning from the stratified period (marked by lack of turbulence) to the ice-off on 3.5.2017 (DOY 123). Time is presented in DOY 2017.

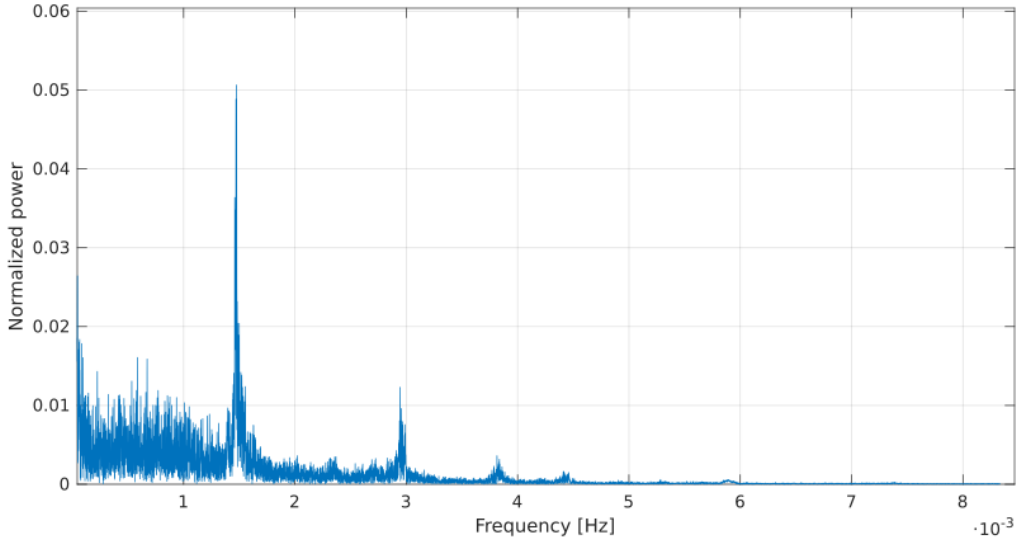


Figure 10: Fourier transform from the $z = 0.5$ m thermistor (northern chain) of a 20 day period (DOY 23 – 43) with clearly visible surface seiche activity. Several peaks can be observed, corresponding to different modes of surface seiche.

The intensities of these peaks diminishes in accordance to the number of the mode, so that higher modes are weaker.

There are other peaks that are possibly the seiche periods of the larger basin (where the instrumentation raft was positioned) or the modes of the east-west direction, but their signal to noise ratios are usually so low that no conclusions can be drawn.

No obvious correlation between high wind speeds or changes in the atmospheric pressure and the amplitude of the seiche oscillations was observed. Also, as the oscillations do not disappear when the ice cover matures and becomes stiffer, it can be concluded that the ice does not prevent, or necessarily hamper at all, the development of barotropic seiches.

Strong, baroclinic waves were observed at least on two occasions, distinguished by their long period. First, there was a wave propagating in the lake when the thermistor chains were deployed (DOY 23), most likely originating from a time when there was no ice cover yet on the lake (Fig. 11). The second event was observed a month and a half later (DOY 69) (Fig. 12).

The first baroclinic wave event could be observed to last for 16 days, or up until DOY 40 with two periods: $T_0 \approx 96.8$ h and $T_1 \approx 48.4$ h according to the wavelet transform of the corresponding isotherms. Both of these have a longer period than would be the inertial period on this latitude (~ 13.6 hours), so they are classified as suprainertial. The wave is of the second vertical mode, which is indicated by the 180° phase difference between the isotherms in the upper and lower edges of the wave (Fig. 13). This wave propagated in the continuously stratified part of the lake, approximately at a depth of $z = 3 - 8$ m. The wave is visible in the isotherm plot of the northern chain, from the

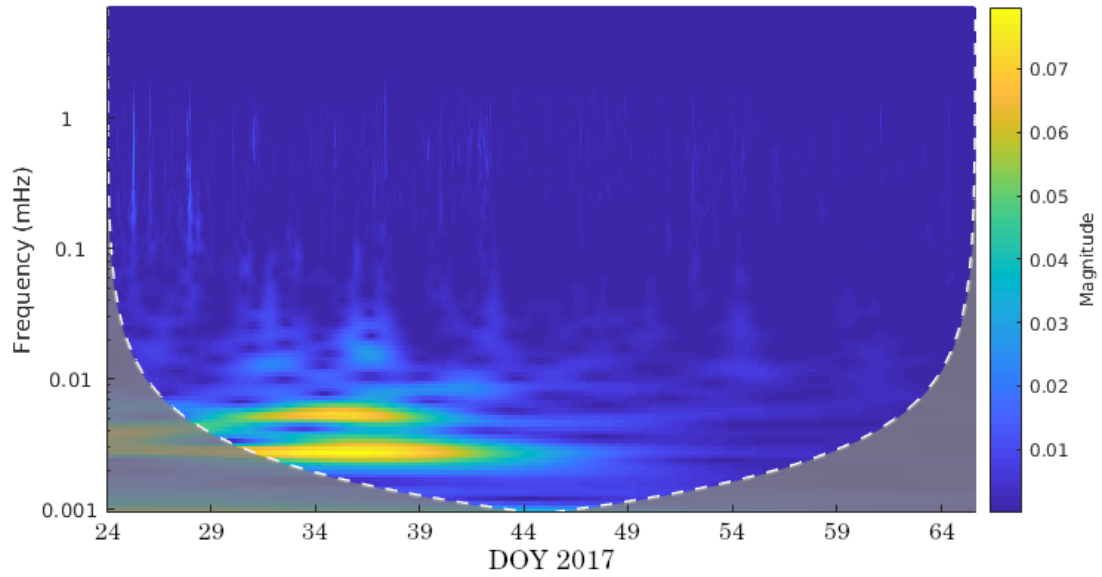


Figure 11: Wavelet transform of the first wave event. Two periods can be seen highlighted in yellow, the top one having a period of 48.4 h and the lower one 96.8 h. The white dashed line indicates the cone of influence, or where the wavelet transform is considered reliable.

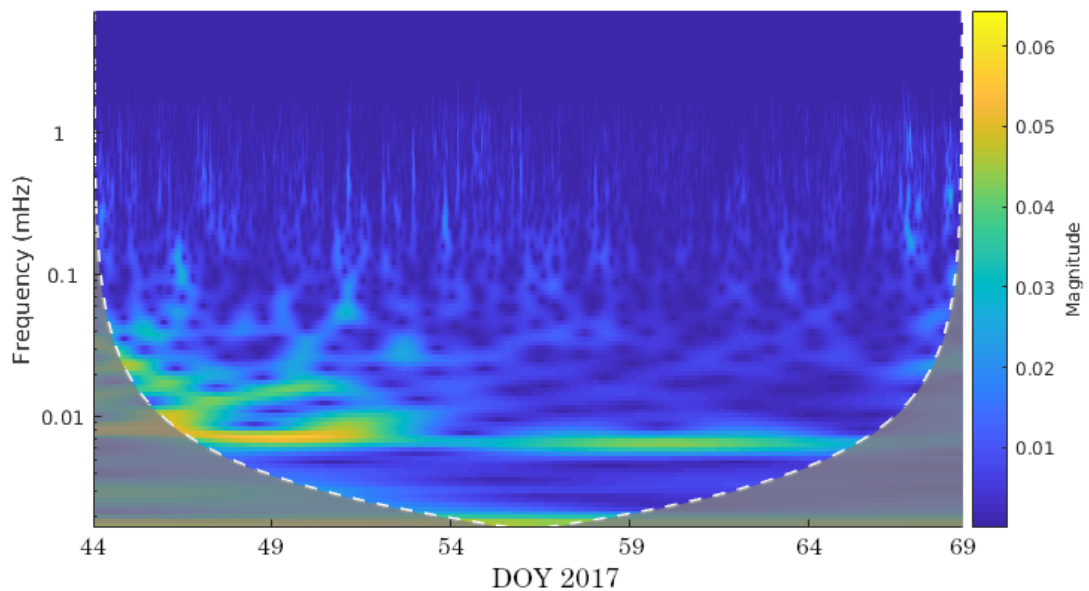


Figure 12: Wavelet transform of the second wave event. The period of the wave is approximately 39.3 h.

start of the measurement period (DOY 23) to DOY 50 (Fig. 14). The two vertical modes are visible for roughly the ten first days of measurements, and after that the wave seemed to propagate as a first vertical mode (V1H1) wave (Fig. 5). Oscillations disappear first from the lower thermocline, and the last oscillations of this event are visible in the upper thermocline. The two other thermistor chains do not show this event as clearly. Both of them show oscillations, but not of the same shape, depth or period as the northern chain. This maybe due to the wave not travelling only horizontally, but vertically as well.

The second baroclinic wave event started approximately on DOY 69 and lasted until DOY 78 (Fig. 12). Its period was $T_0 = 39.3$ h. It is lacking the phase difference that was obvious in the first wave event, so it is of mode V1H1. The wave propagated deeper than the wave of the first event, $z \approx 6 - 8.5$ m. These oscillations are visible in the middle chain (Fig. 15). The amplitude of both of the waves was in the order of tens of centimeters.

To give a further proof that the waves observed were indeed of baroclinic nature, a numerical model to predict frequencies of baroclinic internal seiche modes was employed. The model is outlined in (Münnich et al., 1992), and it is a N-layer model. It assumes a narrow, rectangular basin with a stable stratification. Lake Kuivajärvi fits well for this model, since it is approximately rectangular (Fig. 6). Narrow in this case means that the Rossby radius of deformation (Eq. 21) of the lake is greater than the narrower dimension of the lake. Rossby radius for typical current velocities of a ice covered lake at 62° latitude is in the order of hundreds of meters, which is just about in the limits of lake Kuivajärvi, which is on average around 200 m in width.

For the conditions persisting in the lake in January, which is when the first wave was observed, the model gives a period of approximately 90 h for a second vertical mode, which for considering the limitations of the model, is a close enough result to confirm that the wave indeed was second vertical mode baroclinic seiche in nature.

As was expected, there were waves propagating in the lake for the whole ice-on season. Barotropic surface seiches, and its harmonic modes, were the prominent type of the waves. The first mode was present at all times with varying amplitudes, and various other seiche modes were also visible in the thermistor chain data for most of the time. This was probably partly due to the very elongated and regular shape of the lake, where these kinds of oscillations were free to move and thus their dissipation was slow, in the order of days or weeks.

Baroclinic waves were a bit unexpectedly found in the late winter, under a thick ice cover of over 40 cm. The early winter baroclinic wave event was easy to explain, since it started already during the ice-off season and wind is easily able to excite these waves in the weakly stratified water column. This seems to be confirmed by the numerical model, that gave consistent results for a wave mode that would be expected during the open water season. Under the ice these waves can persist for days, due to the lack of any disturbances and the symmetrical shape of the lake. Late winter internal waves are a bit

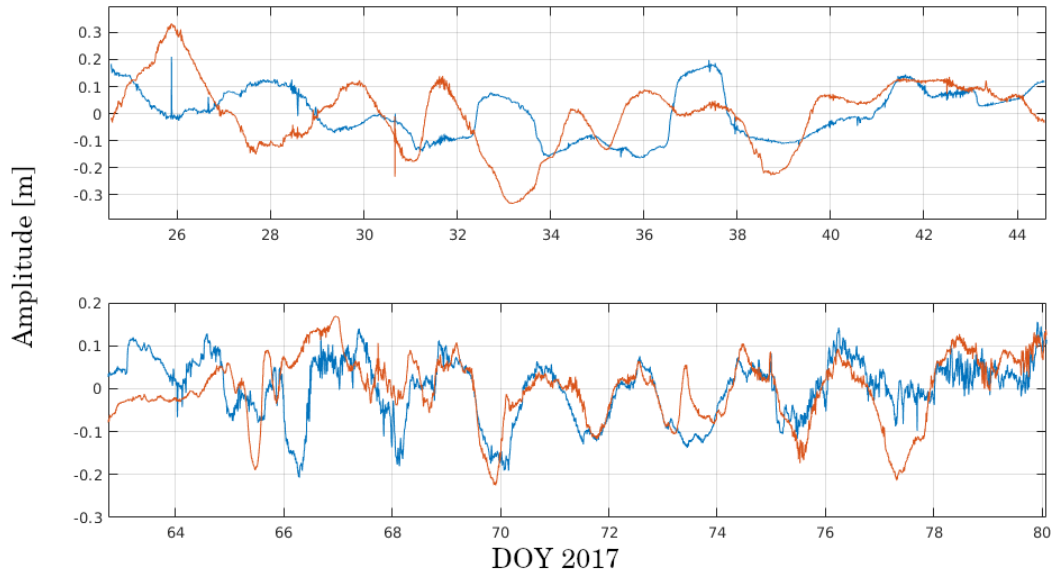


Figure 13: Detrended isotherms from the two baroclinic wave events. The isotherms are taken about one meter apart in z direction. The red lines are higher up from the water column than the blue lines. The first event shows clearly the out of phase nature of the wave, while in latter one the wave is in sync. The amplitude is in the same range in both waves.

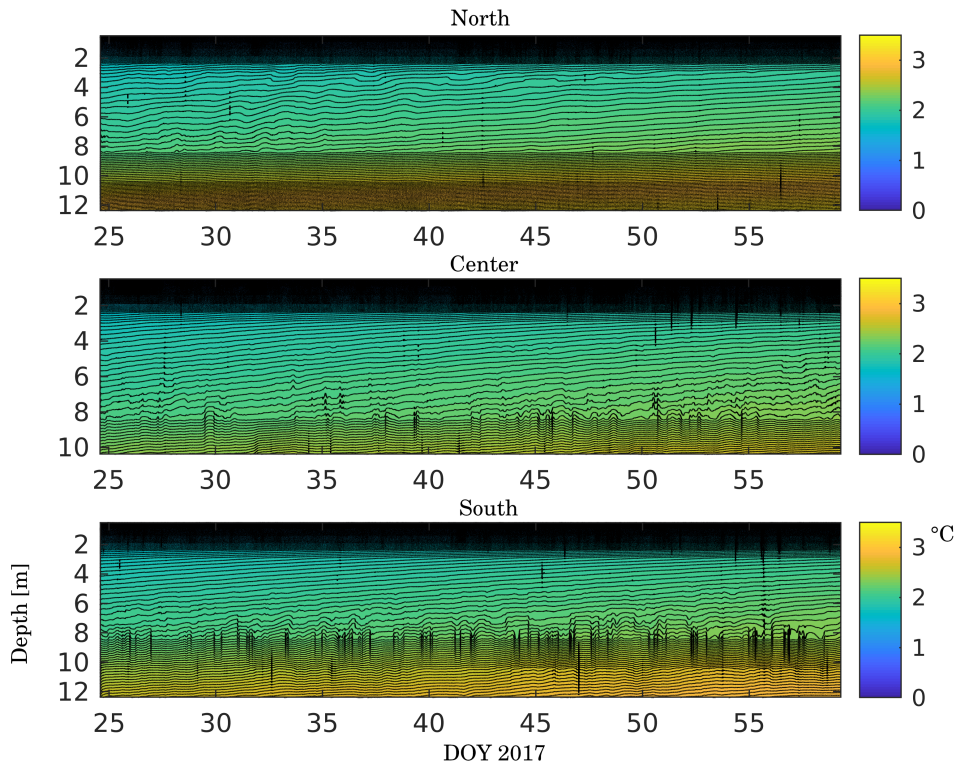


Figure 14: Comparison of the thermistor chain data, interpreted as isotherms. There are 125 isotherms in this plot. Uppermost plot is the northern chain, middle one is the raft chain and bottom one is the southern chain. Y -axis is the depth in meters and x -axis is time in DOY 2017. Colorbar on the right is the temperature in Celsius. Here, the northern chains shows the first wave event between the depths of 2 and 8 m.

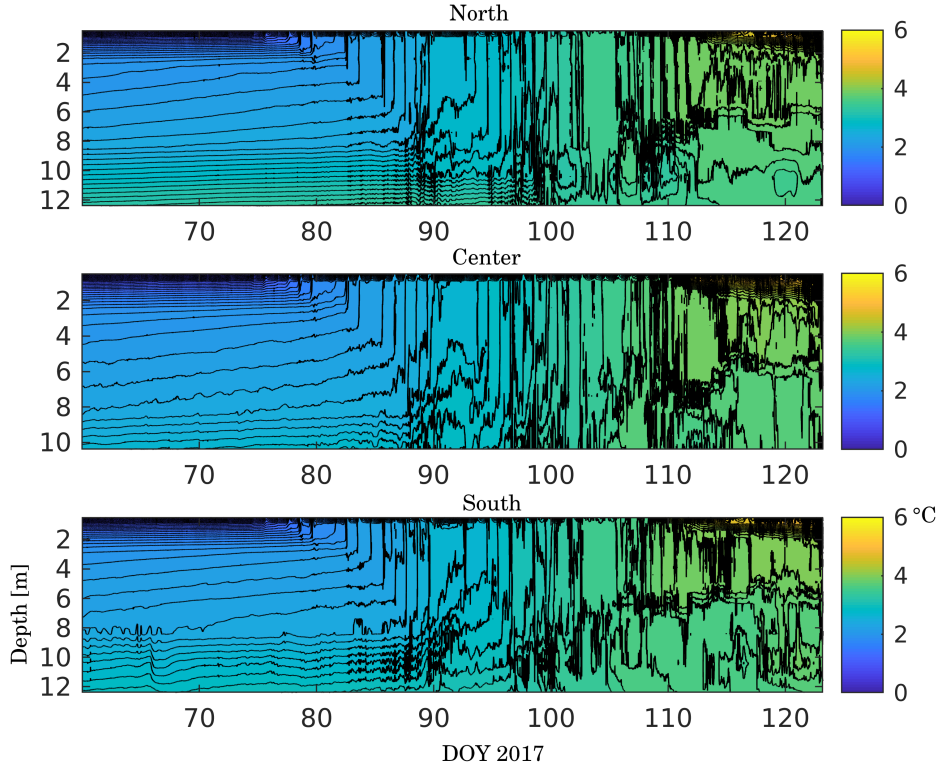


Figure 15: Comparison of the thermistor chain data, interpreted as isotherms. There are 65 isotherms in this plot. Notice, that the scale of the temperature colorbar is different from the previous figure. The second baroclinic wave event is visible in the center chain from the beginning, at a depth of ~ 8 m.

harder to explain, since the thick ice cover is making it difficult for the wind to push the water out of the equilibrium.

One possible way to excite these waves would be an interaction between the water and the ice cover. In a satellite image taken on 17.4.2017 (DOY 87) cracks can be seen on the ice cover (Fig. 16). The formation of these cracks could induce waves by two mechanisms. Either, the cracking of the ice after elastic bending could jolt the water sufficiently, that a wave could be induced. Or secondly, after the crack has been formed, the wind could move the now two pieces of ice cover in such a way, that new waves would be induced. Either way, momentum is transported from the atmosphere into the lake water body.

4.3 Radiation balance

4.3.1 Shortwave radiation and albedo

The noon peak in the incoming solar radiation (Q_s) is very strongly a function of the solar zenith angle, which is evident in the Fig. 17. Also, cloudiness plays an important role in the incoming radiation, and due to that the incoming radiation can plunge late in the spring to levels more typical for mid-winter. The lowest noon peak of Q_s was on DOY 31, when the flux was 30 W m^{-2} , and the highest peak can be found on DOY 122, when

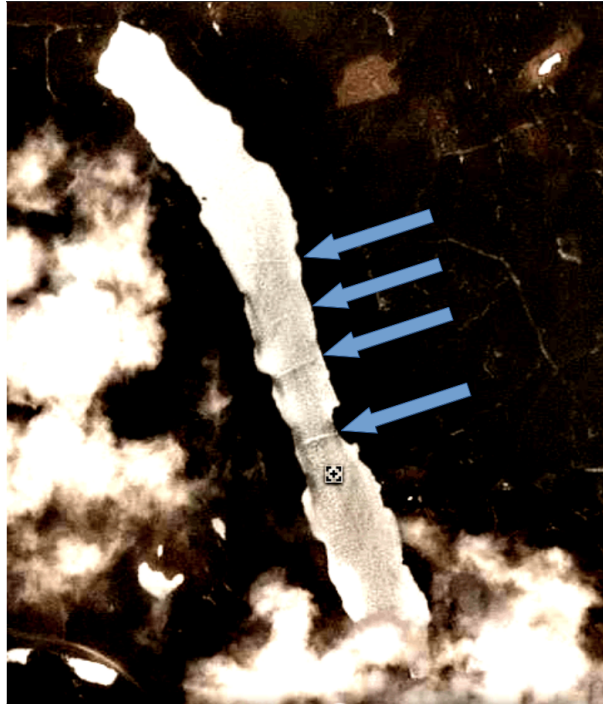


Figure 16: Cracks developed on the ice cover of Kuivajärvi, 17.4.2017. Arrows indicate the cracks, and the crosshair marks the approximate location of the raft. Photo: Planet Labs.

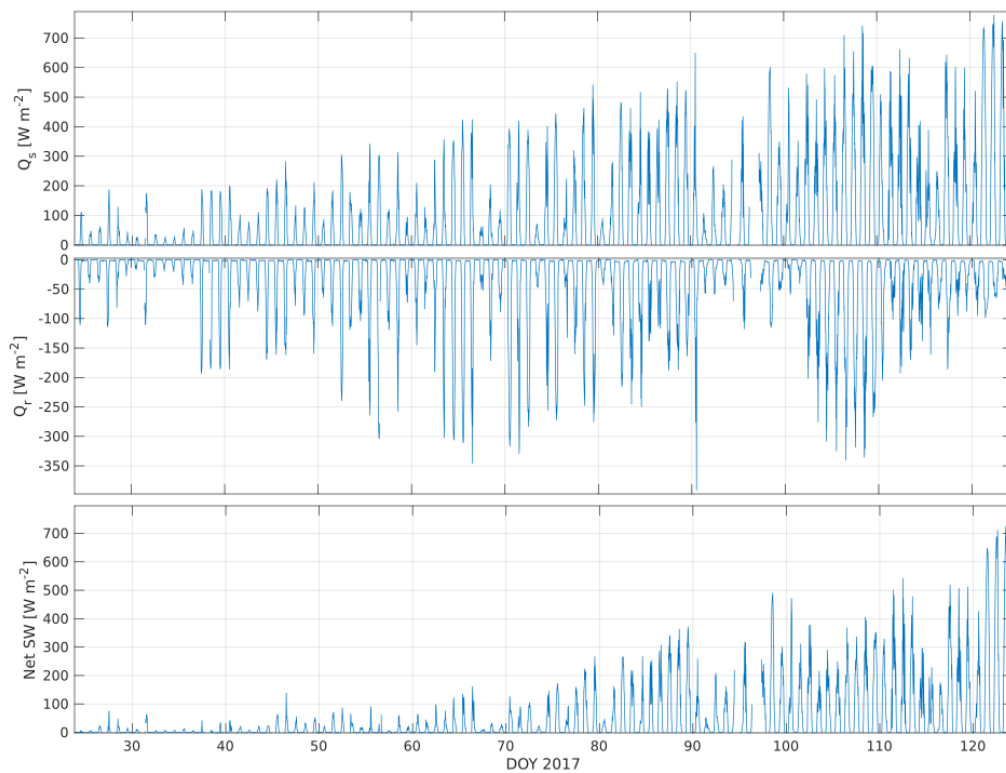


Figure 17: Incoming, reflected and net shortwave radiation over lake Kuivajärvi. A clearly visible trend in the daily peak radiation can be observed in the incoming component. On x -axis is time in DOY 2017.

the flux reached a value of 777 W m^{-2} . In mid-winter thus, the shortwave radiation can

be in the order of the turbulent fluxes, but in the spring it slowly gains a dominant role in the energy balance.

Up until the early March (DOY 70) the albedo stays above 0.5, with fresh snow returning the albedo to values very close to unity (Fig. 18). This is possible due to the fact that in winter the low incoming shortwave radiation is not enough to melt the small snow crystals into larger ones and nearly all of the precipitation is falling down as snow. After DOY 70 these conditions are not met anymore, and the albedo starts a steady decline towards lower values, with only intermittent snowfall returning it to higher values for a short period of time. Just before the ice-off on DOY 122 the albedo has a value very near to zero, meaning that nearly all of the incoming shortwave radiation enters the ice and the water below.

The albedo over the lake has diurnal variation (Fig. 19). It manifests as high value in the morning and evening, with lowest values after noon (Fig. 19). This is due to two factors: First reason is that albedo is an apparent optical property, and as such it is a function of the solar zenith angle. Second, it is also a function of the snow crystals themselves, with bigger crystals having a lower albedo. Melting during the day increases the crystal size, and thus leads to lower albedo as the day progresses (Hadley & Kirchstetter, 2012).

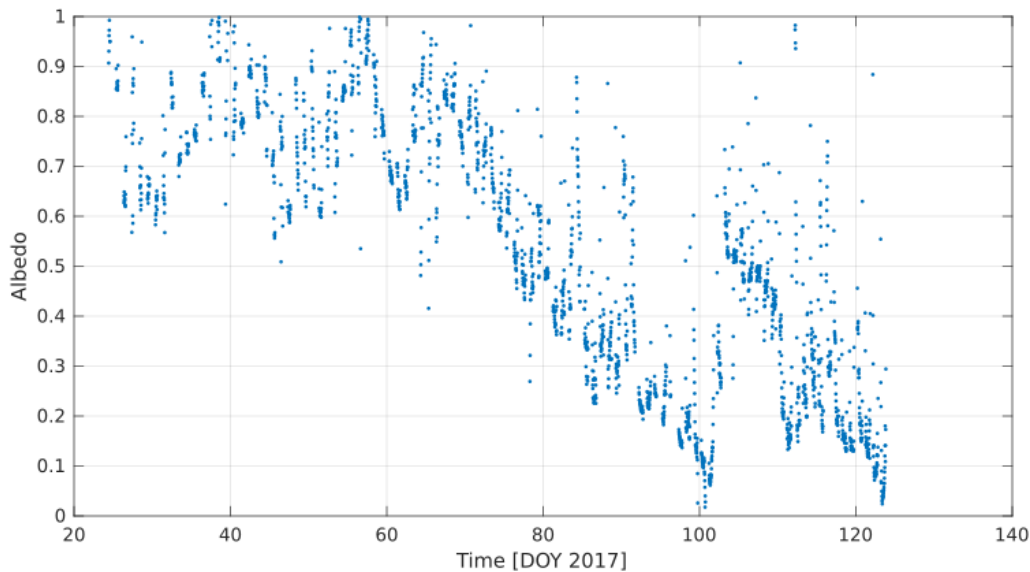


Figure 18: Albedo over lake Kuivajärvi during the ice-on season. During DOY 100 a strong peak in albedo can be seen, which is due to fresh snow falling onto the ice cover.

4.3.2 Longwave radiation

The net longwave radiation is on average throughout the winter negative, i.e. the ice surface loses heat into the atmosphere via terrestrial radiation. Only occasionally is warmer air advected over the lake and the net long wave radiation balance brought up to

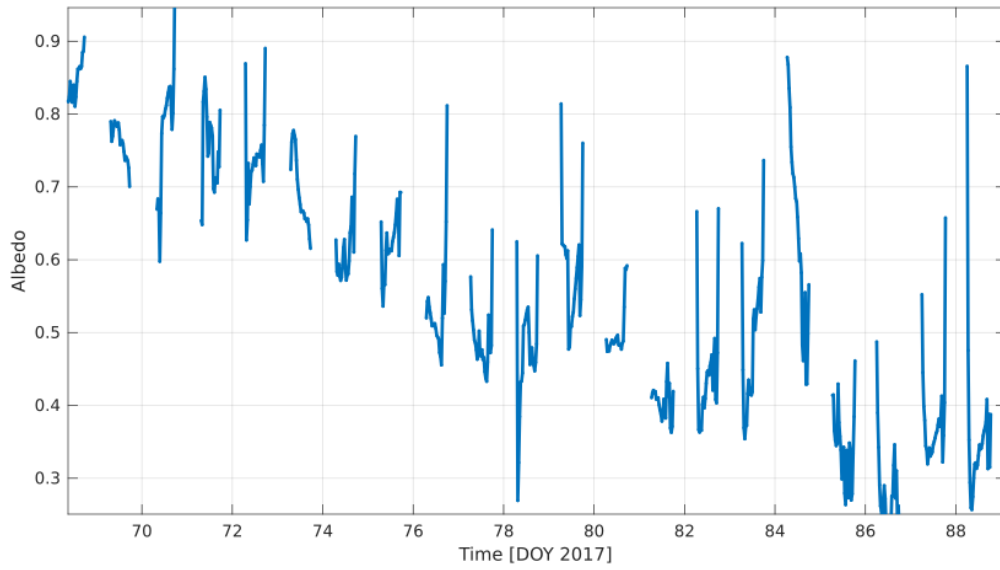


Figure 19: Typical diurnal variation of albedo. At low solar elevations, the albedo is higher than during the midday. This is due to the fact that albedo is an apparent optical property.

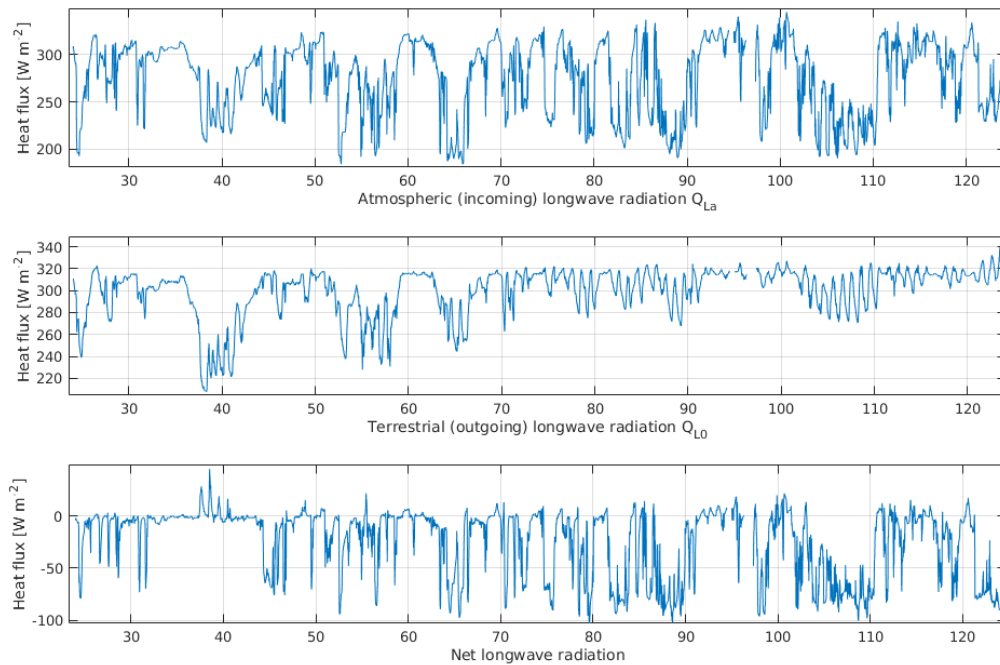


Figure 20: Incoming, outgoing and net longwave radiation. Values of longwave radiation varies rather little throughout the year. On x -axis is time in DOY 2017.

positive values. The mean of incoming, outgoing and net longwave radiation were 271.0, 295.1 and -24.13 W m^{-2} , respectively.

During the melting period, variation in outgoing LW radiation is smaller in comparison to the winter. This is likely due to the ice cover reaching its melting point, and thus having a much more stable temperature, than in the dead of winter. A diurnal variation in amplitude is observable throughout the data set, except occasional periods of thick cloud cover.

4.4 Turbulent fluxes

Sensible heat flux was predominantly negative (heat flux directed towards ice) throughout the ice-on season. Mean value of sensible heat flux was -10.12 W m^{-2} (Fig. 21). This indicates that a situation, where a warm front pushes over the lake ice and brings in heat was more prevalent, than the opposite case.

Latent heat flux mostly took heat from the ice, so the values were predominantly positive (Fig. 21). In winter, this means either sublimation of ice from the snow cover or vaporization of melted snow. Mean value of latent heat flux was 2.46 W m^{-2} .

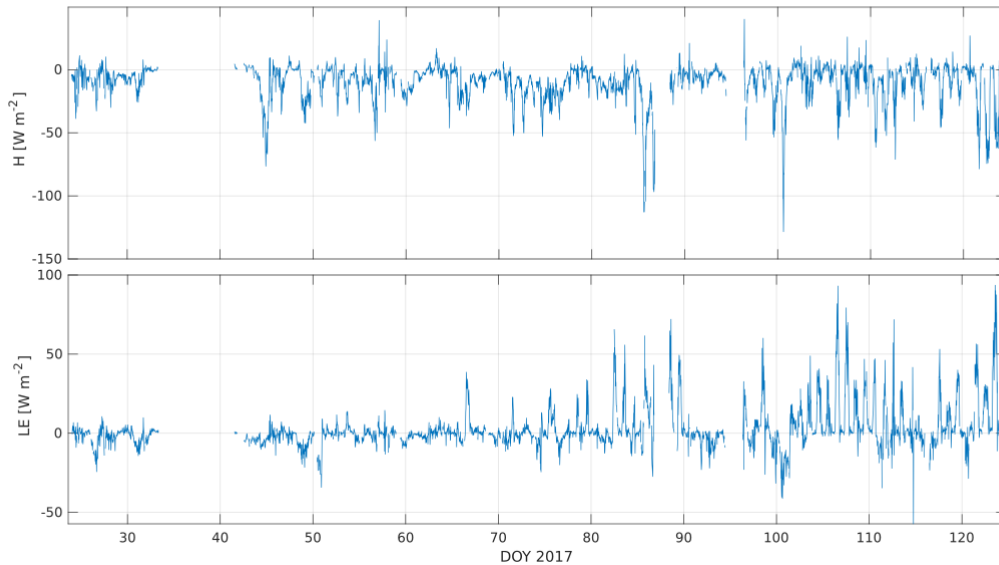


Figure 21: Sensible and latent heat fluxes.

Comparing the results of eddy covariance and bulk aerodynamic method showed that the correlation fairly good (Fig. 22). Squares of their correlation coefficients were $r_H^2 \approx 0.68$ and $r_{LE}^2 \approx 0.72$. The shape of the correlation is not perfectly linear. In sensible heat there seems to be some square dependency that is not taken into account, and in the latent heat flux there are problems especially in the values near zero. The problems with LE arise from two facts: One is that the emissivity of the ice or snow surface changes significantly depending on the situation, and that there is no reliable method to estimate

it. Second problem was the bad calibration of the long wave radiometer, which gave consistently too high values. Combined with the fact that the surface temperature is estimated from the Stefan-Boltzmann law, where it is a function of the fourth root of the outgoing longwave radiation and the emissivity (which was assumed constant), and that the saturation vapor pressure is exponentially a function of this surface temperature (Eq. 25) it is to be anticipated that there will be significant inaccuracies. As the sensible heat flux is only linearly a function of the surface temperature (Eq. 9), the problems are not so evident, but some are still present.

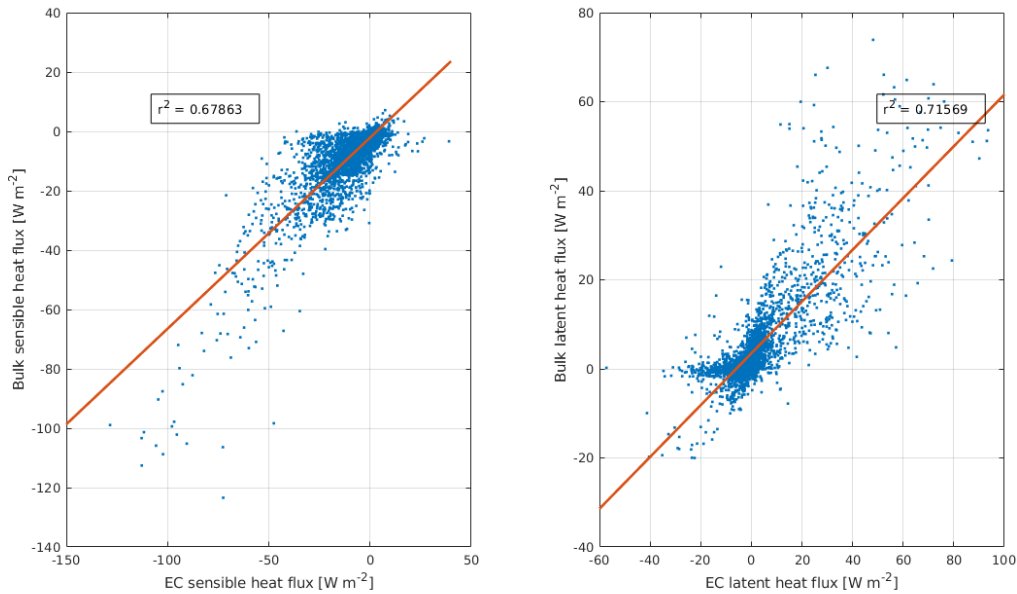


Figure 22: Comparison of EC and bulk aerodynamic method with a linear fit, H on the left and LE on the right. Values of their correlation coefficients squared (r^2) are displayed for both.

4.5 Sediment heat flux

According to the pressure sensors on the sediment thermistor setup, the bottom of the heat flux is calculated at $z = 12.55$ m from the lake surface and the top is 32 cm higher, at $z = 12.23$ m. As expected, the temperature difference between these two sensors decreased rapidly after the winter stratification was achieved. Some high frequency oscillations can be observed in the topmost thermistors, but the three thermistors at the bottom are very stable. This is interpreted as a proof that they are completely buried in the sediment, and any circulation or waves in the water above it has minimal effect on it, and the assumption of only molecular heat transport is accurate. The heat flux is thus calculated to be through the bottom thermistor and the one 10 cm above it. For water at a temperature of $T = 275$ K, a value of $k = 0.5606$ W m⁻¹ K⁻¹ was suggested in (Ramires & Nieto, 1995) as the thermal conduction coefficient. The heat flux presented in figure 23 was calculated according to equation (12).

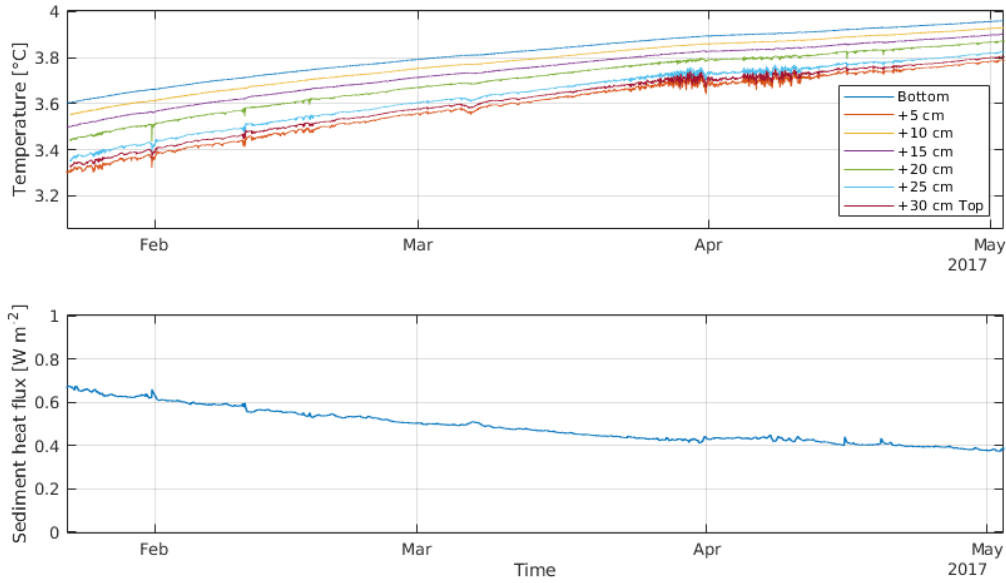


Figure 23: Sediment heat flux and temperature in the sediment during the ice-on season.

From late January onwards, the temperature difference between the top and bottom thermistors was already rather stable at $\Delta T = 0.3^\circ\text{C}$, with a small linear trend. Just before ice-off, the temperature difference was $\Delta T = 0.16^\circ\text{C}$. Right after the winter stratification formed the sediment heat flux Q_{SH} is calculated to be around 2 W m^{-2} (not visible in the plot), at the ice-on it had already decayed to $\sim 0.7 \text{ W m}^{-2}$, and at ice-off it was down to 0.4 W m^{-2} .

4.6 Thermal conditions and stability of the water column

Ice cover formed on lake Kuivajärvi for the first time already in November. This was not the final ice cover of the season, though, as it melted away in a few days. The final ice cover was formed approximately on 20th of January (DOY 20). The thermistor chains were installed on the 24th of January (DOY 24).

The lake had formed a winter stratification at this point. In the first two meters of depth from the ice surface there lied the winter thermocline, characterized by the sharp increase in temperature from the 0°C of the ice / water interface to the little under 2°C of the start of the weakly, but continuously stratified layer. This layer reached to the depth of around $z = 9 \text{ m}$, where the temperature started to increase more rapidly towards the temperature of maximum density in the sediment / water interface. The profile remained this way, accumulating heat via the sediment heating (Fig. 24).

After a period of slow warming in the middle and bottom layers of the lake, the profile beginning on 15th of March (DOY 74) shows the first sign of the breaking of the stratification. It can be seen from the temperature in the winter thermocline increasing, eventually dissolving it into one continuous layer with the weakly stratified layer below it.

The lake was completely mixed all the way to the lowest thermistor ($z = 12.4$ m) by April 13th (DOY 103). On the profile starting on 14th of April (DOY 104) the water column has already begun to build up summer stratification. Ice-off happened on 3.5.2017 (DOY 123).

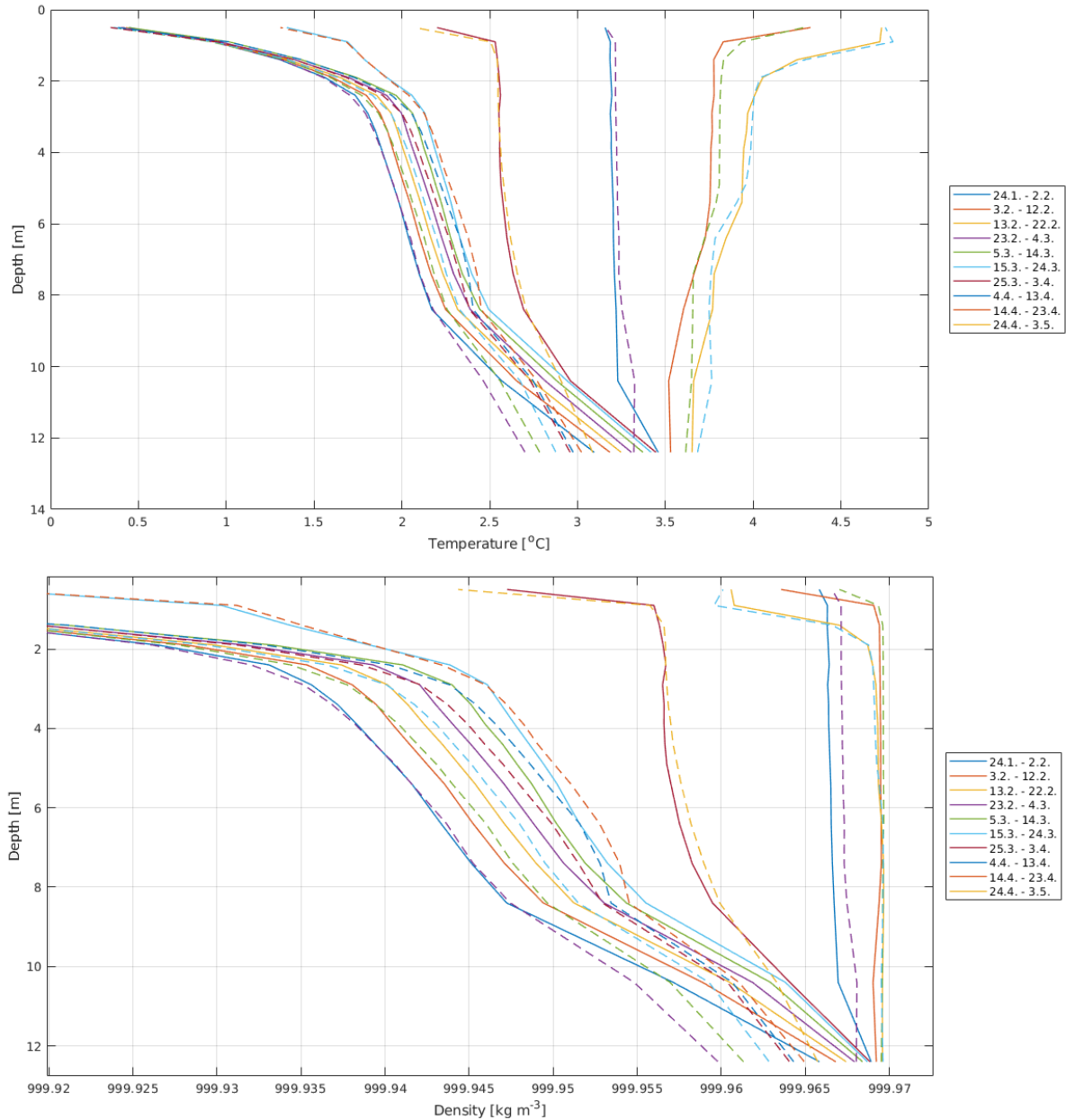


Figure 24: Evolution of the water column temperature and density profiles under ice. Each of the lines represent a ten day average temperature profile. Solid line represents the northern chain, and the dashed lines represent the southern chain.

What is also evident from the temperature profiles is that there is a horizontal density gradient in the lake, possibly due to the uneven sediment heating and variable bathymetry. The gradient of temperature, and thus also density, is sharper on the northern chain than it is on the southern chain. Near the ice / water interface the gradient is very similar, and only very weak horizontal gradient is visible in the continually stratified layer, part of

which could be due to differences in the calibration of the thermistors. This effect is the strongest near the bottom, where one would also expect the biggest effect from uneven sediment heating. The single point measurements done on the sediment heating is not enough to give information about the validity of this hypothesis.

The heat content of lake increases linearly during the mid-winter, when there is very little radiation entering the lake. Also, all of the heat released in the formation of the ice cover can be assumed to be conducted to the atmosphere through the ice cover (Lepäranta, 2015). Thus the accumulation of heat can be assumed to originate from the sediment. This is evident from the energy balance (Fig. 28), where the flux of energy is hovering around zero up until DOY 60, and also from the evolution of the temperature profile (Fig. 24) where the heat can be seen to accumulate into the bottom boundary layer and in the continuously stratified layer. Assuming the heat flux to originate from under the thermistor chain can be misleading, since the sediment heat flux causes mixing in the lake, and the temperature profile in the center of the lake can differ significantly from the shorelines, and thus the spread of heat is not exactly even (Fig. 4). This is supported by the fact that calculating the heat flux between DOY 24 – 60 from the water column heat content, a value of $Q_{SH} = 3.61 \text{ W m}^{-2}$ is acquired, which is significantly higher than was measured from the sediment temperature gradient ($Q_{SH} \lesssim 1 \text{ W m}^{-2}$).

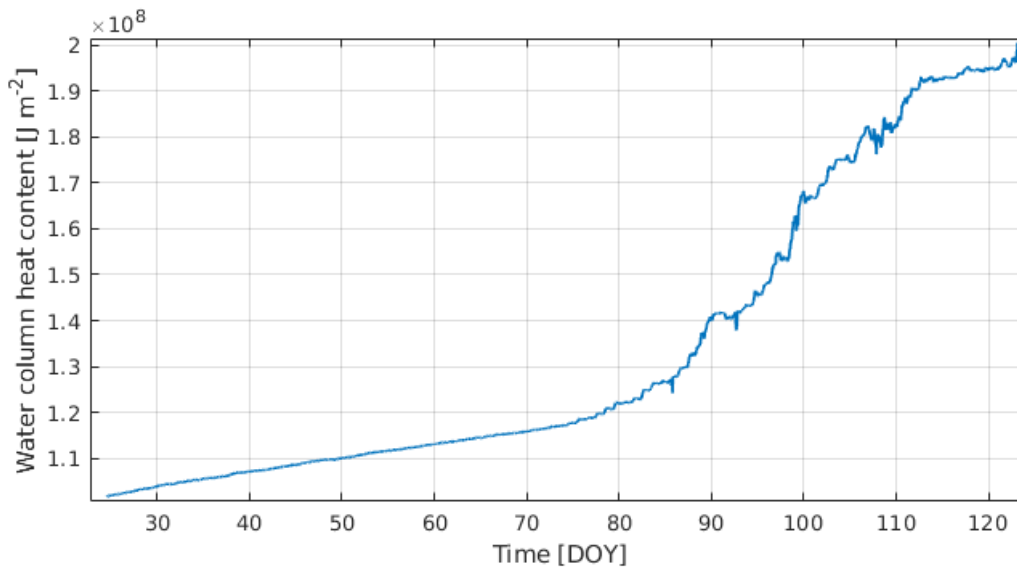


Figure 25: Evolution of the water column heat content ($z = 0 - 12.4 \text{ m}$). The first linear increase in heat content can be attributed to sediment heat accumulation in the lake. Heat content is calculated as deviation from the freezing point.

4.7 Diurnal mixing in spring

In spring, when the surface layer has already been mixed due to the increasing shortwave radiation entering the lake, a diurnal mixing pattern can be seen (Figs. 26 & 27). During the day, SW radiation mixes the surface layer, but during the night, when there is a flux

of heat out of the lake, the surface layer stratifies, although weakly, again. This can be seen to happen from DOY 79 onwards, and happens all the way until the spring overturn on DOY 102.

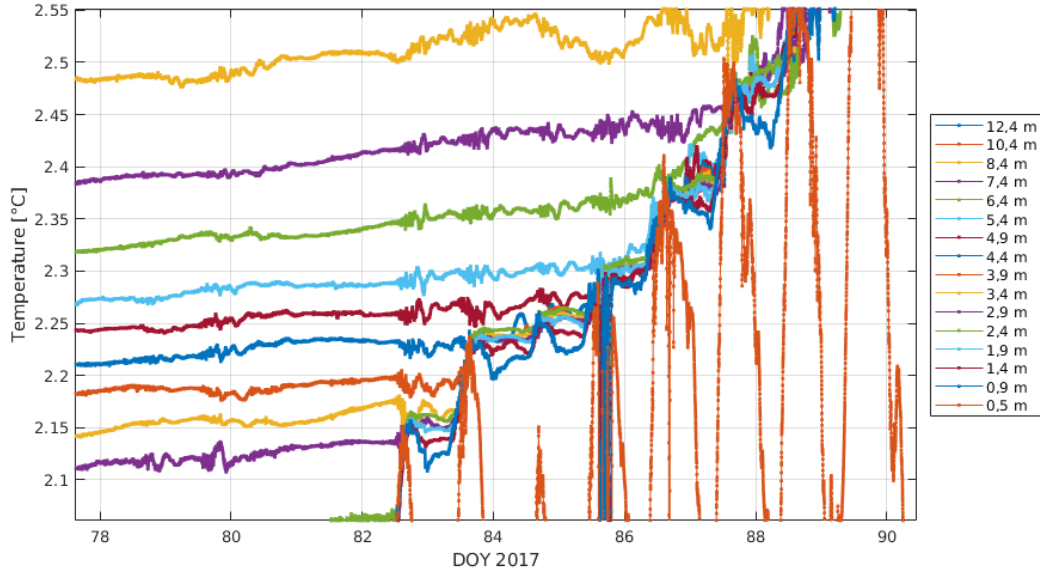


Figure 26: Example of the diurnal mixing pattern during the early spring, northern thermistor chain. The stratification during the night is weak, and the temperature difference in the mixed layer is no more than 0.01 °C. The stratification is at its strongest in the early morning hours, and breaks in the morning with sunlight. Individual lines represent thermistors, with corresponding depths written in the legend.

The daily mixing takes the mixed layer deeper every day. The two topmost thermistors are at the same temperature for the first time on DOY 74, and all of the thermistors are in the same temperature (i.e., spring overturn is happening) on DOY 102. This means that on average the mixed layer thickens by 43 cm per day for the 28 days the penetrative convection happens.

4.8 Energy balance

In Fig. 28 it can be seen, that regarding the energy balance the ice-on season can be divided into two parts: the slightly net negative season where the net radiation balance is very small and the turbulent fluxes play a more significant part and the strongly net positive spring season, when the short wave radiation dominates the balance during daylight hours. There were three periods when the turbulent fluxes were not measured: DOY 33 – 44, DOY 86 – 88 and DOY 94 – 96. This was due to a technical problem with the 3-axis anemometer.

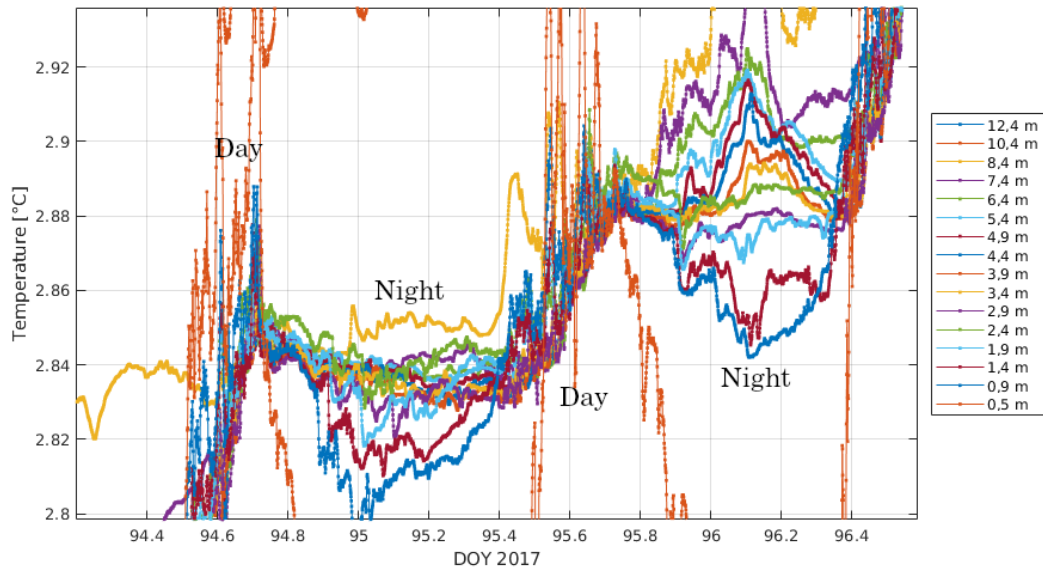


Figure 27: A second example of the diurnal mixing pattern, northern thermistor chain. This is slightly later than Fig. 26, showing how it can stratify nearly the whole water column later on in the spring. Stratification is present when the temperature lines diverge and mixing is present when the lines are packed tightly.

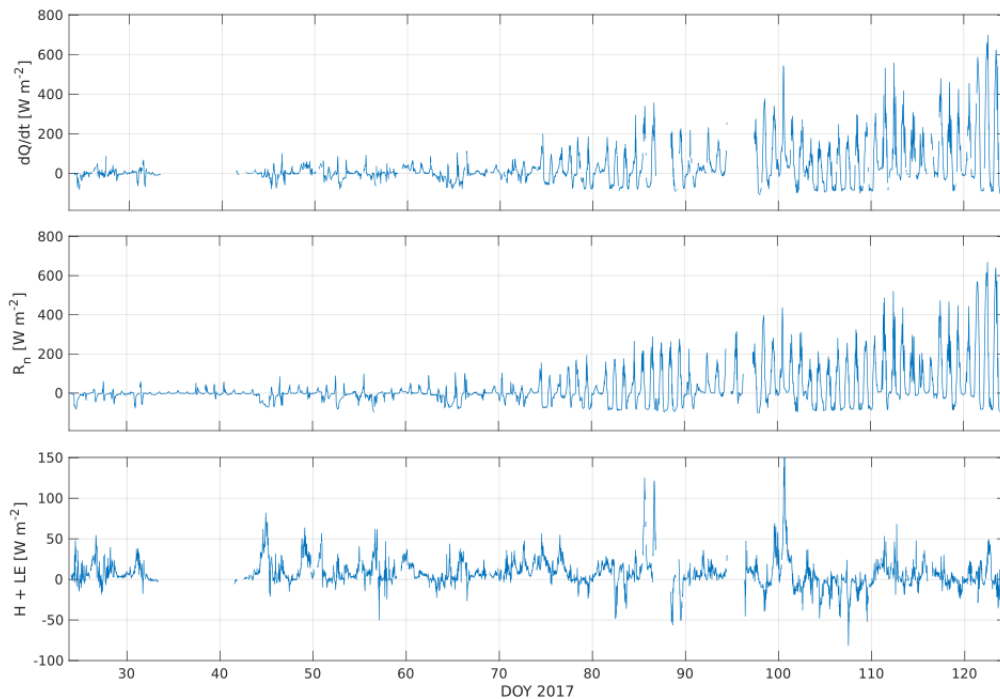


Figure 28: Surface energy balance on lake Kuivajärvi in ice-on season 2016 – 2017. This is the sum of net radiation balance (R_n) and turbulent fluxes ($H + LE$). In the net turbulent fluxes the notation has been changed to correspond to the notation of radiation.

4.9 Ice thickness

As there were rather accurate measurements done on the energy balance, an estimate on the ice growth can be made (Fig. 29). The residual of the sum of all the energy balance components (Eq. (1)) can be calculated, and this can be assumed to be the latent energy of fusion from the formation of the ice cover. It can be compared with the ice thickness measured by the experimental instrument installed on the raft for the winter.

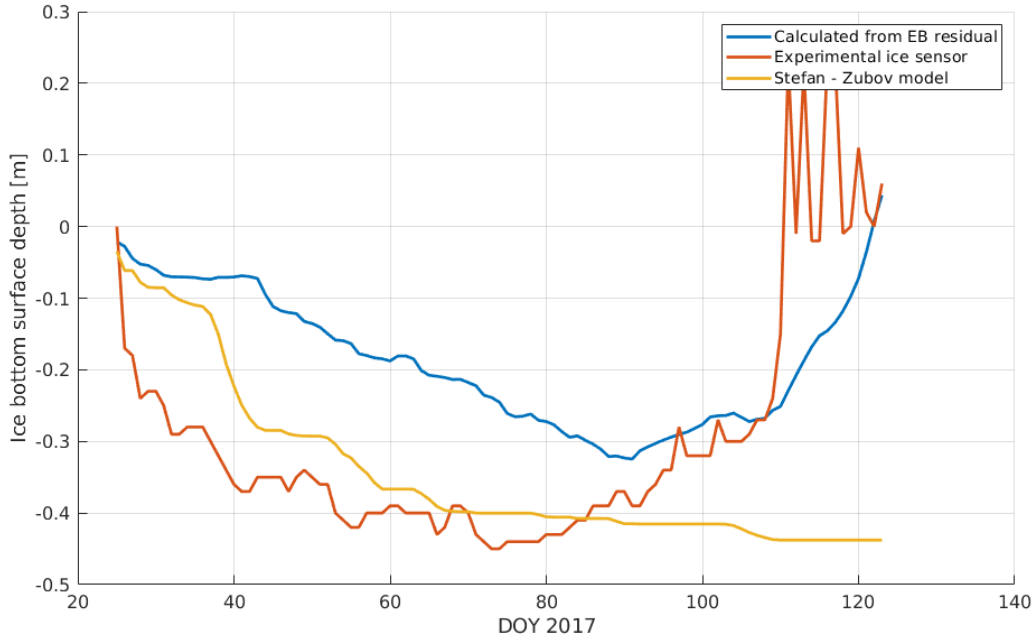


Figure 29: Comparison of the three methods used to evaluate the evolution of the depth of the water / ice interface.

There are several key differences in the two methods of calculating the ice thickness. For one, in the experimental sensor there was no reliable way to discern between snow and ice, so both are included in the thickness. The true ice thickness was around 40 cm at its maximum, so both methods have it pretty close. Melting period is more realistic in the energy balance method, since solar radiation tends to melt ice around the thermistors of the ice sensor, which causes the erroneous values at the end of that data set. Melting starts at different times in these two data sets, with the onset of melting being nearly 20 days later in the EB-computed value. This would mean that the calculation is missing some flux of heat into the lake ice cover. As this lack of heat becomes apparent in the spring, it could be the precipitation heat flux Q_p .

Stefan's law (Eq. 26) only resolves the growth of the ice cover. The resulting ice thickness is in between the previous two methods, although closer to the measured thickness. Modeled melting (or, more accurately, the end of growth) begins nearly at the same time as the measured melting begins, further indicating that some component of the energy balance is not correctly taken into account. This also shows the power of this relatively

simple model to resolve the ice thickness and evolution, although there are differences in the shape of the evolution between the measured and modeled results.

4.10 Precipitation heat flux

Precipitation heat flux proved to be very difficult to estimate. With our current instrumentation it was not possible to always know, whether the precipitation was liquid or solid, or whether the surface was liquid or solid. As the estimation of the surface temperature was based on the longwave radiation, the estimated temperature was very sensitive to the measured LW radiation due to the fourth power in the Stefan-Boltzmann law (Eq. 4). Also, emissivity values are not constant as the surface conditions vary quite radically during the spring, when the likelihood of water phase transition on the surface is at its highest. The estimation of the temperature of the precipitation is also very difficult, and no direct measurement of this was in use.

5 General discussion

There were many types of mixing found in the lake during the ice-on season. These can be divided into two groups: regular (such as the solar radiation, which is defined by the orbital mechanics of our planet and thus is very stable) and unregular (such as internal waves and sediment heating). They are unregular because they are set by the conditions before ice-on or other transient events. Internal waves can be induced before ice-on, and thus the meteorological conditions (mostly wind) persisting over the lake just before ice-on can have significant effect in the water column even weeks after the matter. 'Memory' of the previous summer can be seen in the intensity of the sediment heating.

Comparing the results of turbulent heat fluxes to previous research on a similar lake shows, that there exist some differences in them. In Jakkila et al. (2009) it was shown that the turbulent fluxes would be on average negative throughout the winter (monthly mean values between -8 and 2 W m^{-2} for LE and $-10 - 2 \text{ W m}^{-2}$ for H). Results presented here show more positive values for latent heat flux. They estimated these fluxes with the bulk aerodynamic method, while values over lake Kuivajärvi were acquired by the EC method. This may cause some discrepancy in the results, as in Fig. 22 it can be seen that the bulk aerodynamic method does not represent the EC results perfectly.

Energy balance measurements done on a seasonally ice covered thermokarst lake in Siberia (Franz et al., 2018) showed an almost universally positive values for latent heat flux (mean of 18.6 W m^{-2} for the frozen period). This is different from my results, which show an order of magnitude smaller mean (2.46 W m^{-2}). This could be due to the fact that the air in Siberia is significantly drier, and thus there can be more sublimation of ice and snow. Sensible heat flux in Siberia had a mean of 10.8 W m^{-2} over the frozen

period, which is an almost exact opposite value of what was measured on lake Kuivajärvi (-10.1 W m^{-2}). This could be explained by more cold fronts as opposed to warm fronts that were seen on lake Kuivajärvi.

Daily variation of albedo has been previously reported in (Leppäranta et al., 2010). It showed similar variation than what was observed here, which is to be expected, since the lake in the article (Lake Vendyurskoe in Russian Karelia) is also a boreal lake on a similar latitude.

Estimating the energy balance is difficult due to the widely varying surface conditions. The surface freezes, melts, receives fresh snow and gets flooded by lake water many times over the winter. All of this causes metamorphosis of snow, and thus affects its emissivity and other optical properties. With the current instruments on the raft, it is difficult to reliably quantify the surface conditions. This causes problems with the measurements of the outgoing longwave radiation, and especially in deriving the surface temperature from it. Also, precipitation heat flux was not taken into account in this thesis. Liquid water freezing onto the surface of the ice cover can bring in a heat flux of upwards to 100 W m^{-2} , so it definitely is significant during the spring rains. If no phase transition is occurring, the flux is in the order of a few watts per square meter (Leppäranta, 2015). Quantifying and measuring the effects of precipitation on ice cover and energy balance would be a study of its own, as a model for the rain droplet / atmosphere heat exchange would need to be developed.

Short period surface seiches were observed, and this is in accordance with the previous analysis done on the subject (Kirillin et al., 2012). Long period waves in the winter have been studied very little. One such study was done on a German lake Müggelsee (Kirillin et al., 2009). In it, long period waves were observed, but their periods were very close to the inertial period of the lake suggesting that the rotation of the Earth plays a role in the dynamics. Waves observed in my data were much further away from the inertial period and as such were suprainertial, but showed a similar two peak structure in the early winter wave. Two key differences exist in our analysis, though. First, lake Müggelsee is much more round in its geometry, while lake Kuivajärvi more resembles a channel. Rossby radius is so close to the width of lake Kuivajärvi that it is unlikely that Coriolis would play a part in it, even in the dead of winter. Second, they saw the waves in the sediment / water interface, while the waves observed in lake Kuivajärvi were propagating in the middle of the water column.

Baroclinic internal waves could be studied with more advanced methods. As improvements for the future, the thermistor chains should be positioned further away from each other, in order to have a better picture of what is going on in the lake as a whole. The raft already also includes a thermistor chain, that is able to send data in almost real time, so that any internal waves could be caught as they happen. This would allow for more detailed study to take place, for example to take microstructure profiles to get a more

realistic look at the amount of mixing and turbulence the waves cause. For future, gas measurements (for CO_2 and CH_4) should also be included, in order to see what effect mixing under ice has on the transport of gases into the atmosphere.

Mixing properties of lakes could change if the ice-on season is shortened. As in a weakly stratified lake it is easy to excite internal waves and other forms of mixing, shorter ice-on season means less anoxic conditions in the lake. Warmer waters, more intense mixing and more oxic conditions definitely also affect the gas fluxes and ecology of lakes, something that could and should be better taken into account in upcoming research.

Overall, internal wave and energy balance studies on seasonally ice covered lakes could be expanded, and more data would be useful. One winter is simply not enough to tell, whether the observed phenomena and mean values represent typical conditions.

Acknowledgments

This project took too long. Way too long. That is why I would first like to thank everybody involved in this project for their patience. My supervisor Ivan Mammarella especially showed kindness to me even though the pace was glacial at times, and gave me the generous possibility to work on this data for two summers. Technical staff at the Hyytiälä forestry station helped me significantly as well, by providing well organised and good quality data. Professor emeritus Matti Leppäranta also provided me with valuable insight, which came in handy. Also, professor Petteri Uotila's feedback as a reviewer definitely helped to improve the final quality of this thesis.

The model script that was used in analysing the internal waves was written by Victor Stepanenko, who gave me the permission to use it during his visit in Helsinki. Thanks also belong to him.

My office compatriots Laura Rautiainen, Joula Siponen and Jani Strömberg from the summer of 2018 deserve thanks as well, for being great company during the quiet summer months when this thesis began to take shape.

Thanks also belong to my family Ressu, Timo, Salome and Nora, who have always been supportive of my academic aspirations through the many windings, ups and downs that the last eight years contain, and have provided me with much better sustenance than I could have afforded on my own!

References

- Allen, J.R., 1971: Measurements of Cloud Emissivity in the 8–13 μ Waveband *Journal of Applied Meteorology*, 1971, vol. 10, pp. 260 – 265
- Andreas, E. L., 2005: Handbook of Physical Constants and Functions for Use in Atmospheric Boundary Layer Studies *US Army Corps of Engineers / Engineer Research and Development Center, October 2005*
- Arst, H., Ants, E., Leppäranta, M., Reinart, A., 2006: Radiative characteristics of ice-covered fresh- and brackish-water bodies *Proceedings of the Estonian Academy of Sciences: Geology*, 55(1), p. 3.
- Cohen, E. R., Lide, D. R., Trigg, G. L., 2003: AIP Physics Desk Reference *Springer (New York) & AIP Press (New York)*, p. 357, ISBN 0-387-98973-0
- Dijkstra, H. A., 2008: Dynamical oceanography (Corr. 2nd print) *Berlin: Springer Verlag*. p. 276. ISBN 978-3-540-76375-8
- Franz, D., Mammarella, I., Boike, J., Kirillin, G., Vesala, T., Bornemann, N., Larmanou, E., Langer, M., & Sachs, T., 2018: Lake-Atmosphere Heat Flux Dynamics of a Thermokarst Lake in Arctic Siberia *Journal of Geophysical Research: Atmospheres*, 5 May 2018
- Hadley, O. L., Kirchstetter, T. W., 2012: Black carbon reduction of snow albedo *Nature Climate Change*, vol. 2(6), p. 437 (2012)
- Hampton, S.E., Galloway, A.W.E., Powers, S.M., Ozersky, T. et al., 2017: Ecology under lake ice *Ecology letters*, vol. 20, issue 1, pp. 98 – 111 (2017)
- Hari, P. and Kulmala, M., 2005: Station for Measuring Ecosystem–Atmosphere Relations (SMEAR II) *Boreal Environ. Res.*, 10, pp. 315 – 322, 2005.
- Horn, D.A., Imberger, J., Ivey, G. N., 2001: The degeneration of large-scale interfacial gravity waves in lakes *Journal of Fluid Mechanics*, 2001, vol. 434, pp. 181 – 207
- IOC, SCOR and IAPSO, 2010: The international thermodynamic equation of seawater - 2010: Calculation and use of thermodynamic properties *Intergovernmental Oceanographic Commission, Manuals and Guides No. 56, UNESCO (English)*, 196 pp.
- Jakkila, J., Leppäranta, M., Kawamura T., Shirasawa, K., Salonen, K., 2009: Radiation balance and heat budget during the ice season in lake Pääjärvi, Finland *Aquatic Ecology*, 7.8.2009

- Lee, S., 2014: A theory for polar amplification from a general circulation perspective *Asia-Pacific Journal of Atmospheric Sciences, January 2014, Volume 50, Issue 1, pp. 31–43*
- Leppäranta, M., 2015: Freezing of Lakes and the Evolution of their Ice Cover *Springer-Verlag Berlin Heidelberg 2015*
- Leppäranta, M., Virta, J., Huttula, T., 2017: Hydrologian perusteet *Helsingin yliopisto, Fysiikan laitos 2017, Unigrafia*
- Leppäranta, M., Terzhevik, A., & Shirasawa, K., 2010: Solar radiation and ice melting in Lake Vendyurskoe, Russian Karelia *Hydrology Research, 41.1, pp. 50 – 62, 2010*
- Münnich, M., Wüest, A., Imboden, D.M., 1992: Observations of the second vertical mode of the internal seiche in an alpine lake *Limnology and Oceanography, vol. 37(8), pp. 1705-1719*
- Kirillin, G., Leppäranta M., Terzevik A., Nikolai, G., Bernhardt J., Eneghardt, C., Efre-mova, T., Golosov, S., Palshin, N., Sherstyankin, P., Zdorovenova, G., Zdorovenov, R., 2012: Physics of seasonally ice-covered lakes: a review. *Aquatic sciences Vol. 74: pp. 659 – 682*
- Kirillin, G., Engelhardt, C., Golosov, S., Hintze, T., 2009: Basin-scale internal waves in the bottom boundary layer of ice-covered Lake Müggelsee, Germany *Aquatic Ecology, 2009, 43:641-651*
- Korhonen, J., 2006: Long-term changes in lake ice cover in Finland *Hydrology research, Volume 37, Issue 4-5, 2006*
- Malm, J., 1999: Some properties of currents and mixing in a shallow ice-covered lake *Water Resources Research, vol. 35, issue 1, pp. 221 – 232, January 1999*
- Merian, J. R., 1828: Ueber die Bewegung tropfbarer Flüssigkeiten in Gefassen *Schweighauser (Basel), 1828*
- Phillips, O. M., 1970: On flows induced by diffusion in a stably stratified fluid. *Deep-Sea Research, Vol. 17: s. 435 – 443*
- Puhakka, T, Bister, M., 1996 & 2005: Dynamiikka I – Ilmakehän termodynamiikka *Helsingin yliopisto, Meteorologian laitos, 1996*
- Ramires, M.L.V., Nieto, C.A., 1995: Standard Reference Data for the Thermal Conductivity of Water *Journal of Physical and Chemical Reference Data 24, 1377 (1995)*

- Rizk, W., Kirillin, G., Leppäranta, M., 2014: Basin-scale circulation and heat fluxes in ice-covered lakes *Limnology and Oceanography* Vol. 59(2): pp. 445 – 464
- Rogers, R. R., Yau, M. K., 2014: A Short Course in Cloud Physics (3rd ed.) *Pergamon Press*. p. 16. ISBN 0-7506-3215-1
- Vidal, J., Casamitjana, X., Colomer, J., Serra T., 2005: The internal wave field in Sau reservoir: Observation and modeling of a third vertical mode *Limnology and Oceanography*, 50(4), 2005, 1326 - 1333
- Wunsch, C., 1970: On oceanic boundary mixing. *Deep-Sea Research*, Vol. 17: pp. 293 – 301